AD-A078 719 NORTH CAROLINA STATE UNIV RALEIGH SOLID STATE ELECTR--ETC F/G 20/12
A THEORETICAL SEARCH FOR SUPER-VELOCITY SEMICONDUCTORS.(U)
DEC 79 M A LITTLEJOHN , J R HAUSER N00014-76-C-0480

UNCLASSIFIED NL

| OF |
AD A078719

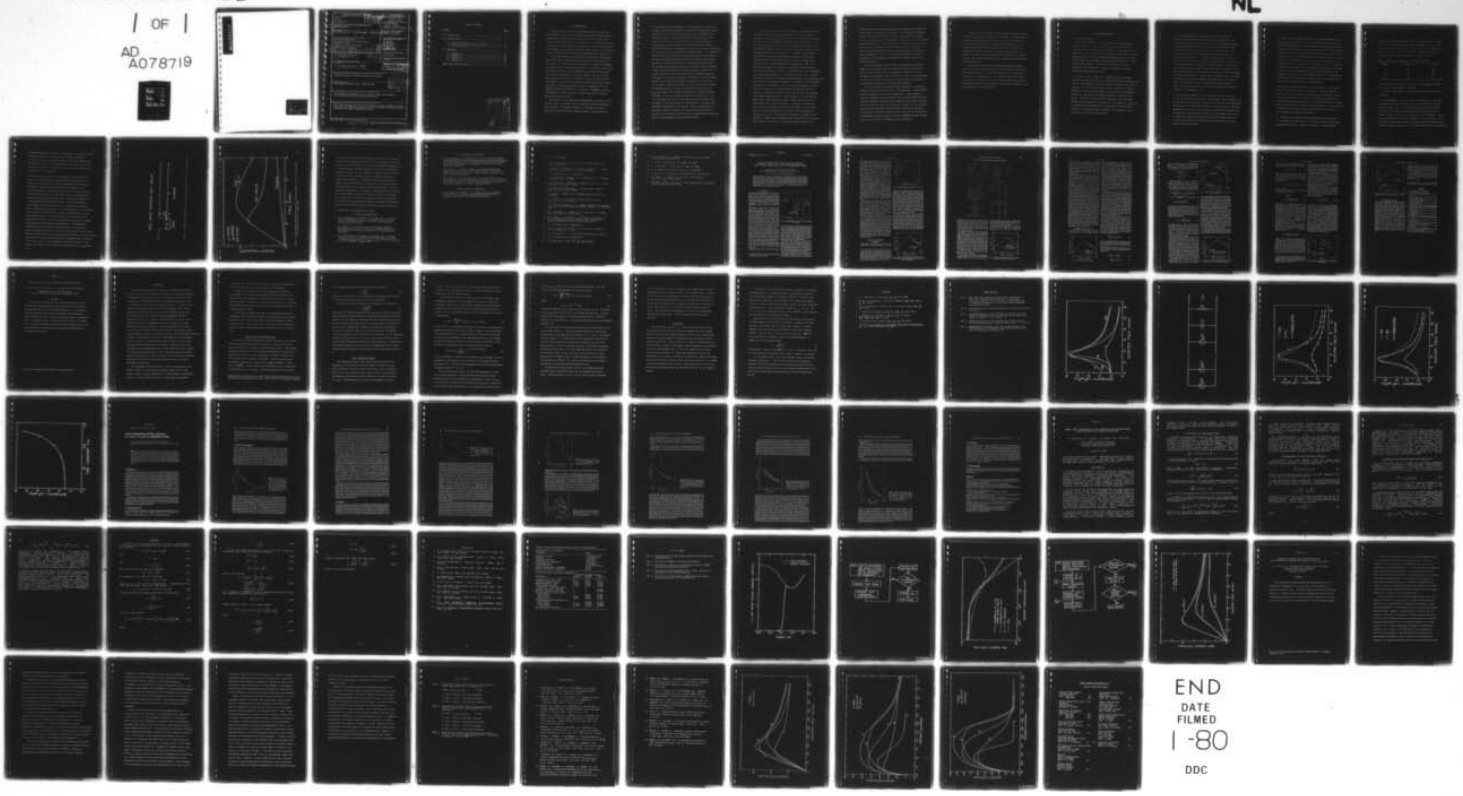

END
DATE FILMED
1-80
DDC

SECURITY CLASSIFICATION OF THIS PAGE (When Data Entered)

REPORT DOCUMENTATION PAGE

READ INSTRUCTIONS BEFORE COMPLETING FORM

1. REPORT NUMBER
ONR-TR-

2. GOVT ACCESSION NO.

3. RECIPIENT'S CATALOG NUMBER

4. TITLE (and Subtitle)
A THEORETICAL SEARCH FOR SUPER-VELOCITY SEMICONDUCTORS

5. TYPE OF REPORT & PERIOD COVERED
Technical-Annual
1/1/79 - 12/31/79

6. PERFORMING ORG. REPORT NUMBER

7. AUTHOR(s)
M. A. Littlejohn, J. R. Hauser and T. H. Glisson

8. CONTRACT OR GRANT NUMBER(s)
N00014-76-C-0480

9. PERFORMING ORGANIZATION NAME AND ADDRESS
N. C. State University
Department of Electrical Engineering
Raleigh, NC 27650

10. PROGRAM ELEMENT, PROJECT, TASK AREA & WORK UNIT NUMBERS
PE 61153N
RR 021-02-03
NR 243-006

11. CONTROLLING OFFICE NAME AND ADDRESS
Office of Naval Research

12. REPORT DATE
December 1979

13. NUMBER OF PAGES
Annual rept. 1 Jan - 31 Dec 79

14. MONITORING AGENCY NAME & ADDRESS(if different from Controlling Office)
RR 021 02

15. SECURITY CLASS. (of this report)
Unclassified

15a. DECLASSIFICATION/DOWNGRADING SCHEDULE

16. DISTRIBUTION STATEMENT (of this Report)
RR 021 02 03

DISTRIBUTION STATEMENT A
Approved for public release;
Distribution Unlimited

17. DISTRIBUTION STATEMENT (of the abstract entered in Block 20, if different from Report)
Approved for Public Release; distribution unlimited.

DDC RECEIVED DEC 27 1979 A

18. SUPPLEMENTARY NOTES
ONR Scientific Officer; Tel. (202) 696-4218

19. KEY WORDS (Continue on reverse side if necessary and identify by block number)
III-V Compound semiconductors, III-V Alloys, High-Field Transport, III-V Semiconductor Devices, Microwave devices.

20. ABSTRACT (Continue on reverse side if necessary and identify by block number)
This report presents the results of research on carrier transport in III-V semiconducting compounds and alloys and the performance of microwave devices fabricated from those compounds and alloys.

DD FORM 1 JAN 73 1473 EDITION OF 1 NOV 65 IS OBSOLETE

411511

SECURITY CLASSIFICATION OF THIS PAGE (When Data Entered)

TABLE OF CONTENTS

1.0 INTRODUCTION

During the past five years an ONR-sponsored research program has been underway in the Electrical Engineering Department at North Carolina State University which basically involves the use of the Monte Carlo method to study high-field transport properties of semiconductor materials. The emphasis has been directed toward the study of ternary and quaternary III-V compounds in an attempt to identify specific materials with desirable electronic properties for microwave and high-speed device applications.

A substantial effort has been devoted to developing a comprehensive Monte Carlo computer program which can be used as a predictive tool in the study of hot electron transport, as well as low field ohmic transport, in a general class of semiconductor materials. We presently believe that the capabilities which have been developed so far under ONR sponsorship are second to none within the scientific community, and that the bulk static transport properties of two general classes of quaternary III-V semiconductors can be predicted using our computational methods. These two classes of quaternary materials consist of compounds of the form $A^{III}_{1-x}B^{III}_{x}C^{V}_{1-y}D^{V}_{y}$ and $A^{III}_{x}B^{III}_{y}C^{III}_{z}D^{V}$ (or conversely $A^{III}B^{V}_{x}C^{V}_{y}D^{V}_{z}$), which can be specified to include any binary or ternary compound as a subset of these general material forms.

The accuracy of the computational program depends on several factors. One major factor is the way in which the quaternary material parameters are calculated. The technique depends on a knowledge of the binary material parameters and either theoretical models or experimental data

for the ternary material parameters. This information is coupled into a general interpolation procedure for calculating the quaternary material parameters, from which the transport properties are obtained in the Monte Carlo method. This work resulted over three years ago in the prediction that specific compositions of the quaternary compound $Ga_{1-x}In_xP_{1-y}As_y$ lattice-matched to InP substrates possess transport properties having distinct advantages over GaAs [1] for device applications. In the past three years considerable experimental work on this compound has shown the material to indeed be promising for many device applications, although the principal applications have been for electrooptic devices. However, the complete advantages due to the predicted superior transport properties have not been realized at the present time, and efforts to make a microwave MESFET have only been partially successful [2]. It appears that many of the device problems can be overcome through the refinement of the materials technology, and there are reasons to remain optimistic that the predicted material advantages will be realized. In the authors' opinion the influence of alloy scattering still remains an unanswered question. However, recent results on $Ga_{1-x}Al_xAs$ and $Ga_{1-x}In_xAs$ suggest that our approach which uses the electron affinity difference for the alloy scattering potential is correct [3]. It is to be noted that these recent results have come about through careful refinement of the growth process in these materials to the point where reasonably pure material can be achieved. Then, by examining the low temperature (77K) Hall mobility, the effects of alloy scattering in $Ga_{1-x}Al_xAs$ can be separated from those due to ionized impurity scattering, and are in good agreement with our previous models.

In contrast to these results very little basic information has been accumulated which elucidates experimentally the electron transport properties of $Ga_{1-x}In_xP_{1-y}As_y$ which will directly determine its usefulness as a material for high-frequency, high-speed device applications. From our own laboratory work in the growth of the quaternary it appears that many material problems remain to be solved before the true nature of the transport properties can be elucidated. For example, energy bandgap measurements do support the interpolation procedure for determining quaternary material energy bandgaps [4-6]. However, measurements of effective mass by various techniques are contradictory. Some of the measurements support the interpolation [6,7] while other experimental data are contradictory to it [8,9]. In addition, Hall effect measurements of the temperature dependence of the electron mobility [10,11] indicate that alloy scattering is considerably more prominent than is predicted by even the largest of the theoretical estimates. In addition, for the quaternary compositions lattice-matched to InP it has been very difficult to form Schottky barriers on n- or p-type material [2], and there are often problems in forming rectifying p-n junctions by LPE [12]. The emerging data strongly suggest regions of non-stoichiometric or conducting-type defects which affect the barrier region. Recent experiments in InP grown by MBE [13,14] show the presence of conducting In precipitates which affect the transport properties and the formation of Au-Schottky barriers on InP in a manner which is similar to the measurements on $Ga_{1-x}In_xP_{1-y}As_y$ [15]. The question of the behavior of impurities, the formation of impurity-defect complexes, and the behavior of non-stoichiometric defects is emerging as a significant research problem in the

III-V materials which will greatly affect the experimental and theoretical interpretation of the transport properties. We are beginning to examine ways to study such problems with the Monte Carlo method, for example by initially including the Seitz dislocation scattering in the calculation [16]. The general purpose of the above discussion is to show that at the present time there is not adequate evidence to either confirm or disprove the basic interpolation procedure used for predicting ternary and quaternary material parameters. In fact, as experimental information continues to be gathered, the interpolation procedure can be refined to make it more generally applicable.

We have continued during this year to examine the general area of submicron device physics, and have emphasized the effort to establish physical processes which effect the operation of small devices and to incorporate such mechanisms into the Monte Carlo method. We are examining the limits of the Monte Carlo method, and other transport techniques, as to their general applicability to small device phenomena.

As a first step in this approach we have implemented a conventional transient or step-field approach [17] to examining what is commonly called velocity overshoot in the electron dynamics [18]. Another approach, called the "ensemble" Monte Carlo method, has also been implemented which critically examines various estimation schemes for the dynamical behavior of both electron drift velocity and electron diffusion. We are continuing to consider and investigate other areas such as fluctuation phenomena, modifications of collision interactions and interaction time field effects, two-dimensional material and device effects, fundamental frequency limitations, and the influence of degenerate carrier statistics.

In addition, we have begun to examine electron transport in quasi-two dimensional systems or superlattice structures. We believe that this emerging area has important applications for new device concepts and structures, and that the basic electron transport properties can be very conveniently studied by the Monte Carlo method. Indeed, some of the important phenomena can only be studied by this technique. In addition, the study of electron transport in these types of structures requires a more complete knowledge of the sub-micron related phenomena mentioned previously.

A major goal of this research program is to examine the Monte Carlo method and its general applicability to the study of small device physics and phenomena. It is strongly believed that of the possible techniques to be appropriate for such studies the Monte Carlo method will again, as in the past, prove to be the more complete and accurate computational method to study transport and hot electron phenomena in the next generation of electron devices.

2.0 RESEARCH RESULTS

2.1 Review of Progress

This section contains a brief discussion of the work performed during the past year. Some of this work represents the conclusion of efforts begun more than a year ago, and these are presented here for completeness. Also, a discussion of recently initiated work is included. During the past year we have attacked some problems which were felt as barriers toward the development of the Monte Carlo method for the study of small device effects. Included in this section is a list of publications and presentations. Finally, the appendices include manuscripts published during the year.

1) The work on central $\Gamma(000)$ valley negative resistance has been completed and published recently in Solid-State Electronics (Appendix 4.1). This work is mentioned here because it has basic importance for velocity overshoot. We have studied velocity overshoot in materials which are dominated by central valley transport, and a paper will be prepared for publication. This particular phenomena could be a useful effect for devices. However, the materials growth techniques for the materials probably are not adequately developed, since, for example, $Ga_{1-x}In_xP_{1-y}As_y$ is a material which is dominated to a large extent by central-valley transport. The phenomena cannot be studied in the quaternary at this time because of materials growth problems.

2) We have examined carefully and critically the definitions of estimators for the diffusivity at high electric fields in GaAs. The reasons for this are due, first, to the very large disagreement between the measured diffusivity for electrons in GaAs by the time-of-flight technique [19] and theoretical Monte Carlo calculations [20]. This basic disagreement has not been satisfactorily answered (e.g. see references in Appendix 4.2). Secondly, it appears that as one goes to the small device dimensions diffusion will become more and more important as a possible physical limitation to device performance. Thus, we felt that it was important to establish once and for all the validity of the Monte Carlo method for the calculation of high-field diffusion coefficient in compound semiconductors. This has been accomplished, since it has been concluded that the large discrepancy between experiment and theory is due to unaccounted for circuit effects in the original experiment. A paper on this problem has been accepted for publication in Solid State Electronics (see Appendix 4.2).

3) The theoretical modeling of alloy scattering has been continued, and another paper on this subject has been published recently (Appendix 4.3). At the present time we can only conclude that an alloy scattering mechanism, or some other form of scattering similar to alloy scattering is essentially dominating the transport in the quaternary, and we are investigating other mechanisms for their effects [13]. This work will continue since we have an experimental program dealing with the growth and characterization of the quaternary, and the data obtained in this program will be examined using our theoretical models.

4) We have also been examining the effective mass interpolation in the $Ga_{1-x}In_xP_{1-y}As_y$ system, in an effort to explain the contradictions with experimental effective mass values obtained by Shubnikov-de Hass oscillations (see Introduction). We are presently exploring the possibility that a basic error has been made in extracting effective mass values from the experimental data. Our initial results show that the correction required to extract the band-edge effective mass from the mass measured at the Fermi energy at 4.2 K is much larger than reported. Thus, the band-edge corrected effective masses are much smaller than originally reported and are much closer to the interpolated values than the experiments have originally indicated. We have collaborated with Drs. J. B. Restorff and Bland Houston at the Naval Surface Weapons Center on this problem, and we plan to submit a publication in the near future.

5) The work begun almost two years ago on the inclusion of the Pauli Exclusion Principle in the Monte Carlo method is nearing completion, and a paper is in the process of being completed and submitted for publication (see Appendix 4.4). The method is somewhat more general than previous attempts, and has been used to calculate low-field drift mobility, low-field Hall mobility, and high-field drift-velocity. We view this work as the first step toward including electron-electron interactions as a basic mechanism in the Monte Carlo method.

6) The Monte Carlo program has been modified to allow the addition of a sinusoidal (in time) electric field and the calculation of mobility (amplitude and phase) as a function of frequency. Some preliminary

results have been obtained for GaAs. For a dc (bias) field E_o = 1 kV/cm and a 10 GHz ac field with peak amplitude 200 V/cm we find $\mu_{ac} \simeq 7133$ in good agreement with the value $\mu_{dc} = 7284$ obtained from the standard (dc) Monte Carlo program. For E_o = 7 kV/cm (i.e., biased in the negative resistance region) we obtained the results in Table 1 below.

Table 1. Mobility vs frequency for n-GaAs ($N_i = 10^{16} cm^{-3}$).

f(GHz)	$\lvert\mu\rvert$ ($cm^2/v \cdot s$)	$\angle\mu$ (deg)
10	288	160°
50	267	147°
100	202	85°

These data are described reasonably well by a simple single pole model with a corner (-3dB) frequency of 100 GHz.

We shall continue these studies and publish the results during the coming year.

7) The investigation of transient (step field) response is continuing. An "ensemble" Monte Carlo program is used to compile carrier histories (position, energy, etc.) from which the spatial distribution, k-space distribution, and various instantaneous ensemble averages (velocity, energy, position, variance of positions, etc.) can be determined. Results have been obtained for n-GaAs ($N_i = 10^{16} cm^{-3}$) for step fields E = 1, 4, 7, and 20 kV/cm representing the ohmic, threshold, negative resistance, and saturation regions, respectively, of the static velocity-field characteristic.

A paper describing these results is in preparation. In addition, we have examined the influence of effective mass on velocity overshoot in $Ga_{1-x}In_xP_{1-y}As_y$ and have published a paper on this work (Appendix 4.5). The conclusions of this paper demonstrate the real need to resolve the question of the validity of the interpolation procedure for predicting effective mass in the quaternary.

8) We have initiated a study of the phenomena of real-space electron transfer, which is a concept originated by Hess and Streetman at the University of Illinois [21]. The work performed here has been done in collaboration with this research group and is proving to be a very fruitful interaction. Real space electron transfer involves the use of layered heterostructures of the type recently used to study modulation doping in superlattice-type materials [22]. The structures employ a set of alternating lattice-matched semiconductor layers with dissimilar energy bandgaps and electron mobilities, as schematically depicted in Figure 1 using GaAs and $Ga_{1-x}Al_xAs$. For an applied electric field parallel to the interface, the electrons are initially primarily located in the high mobility material. As the field increases the electrons can be thermionically emitted into the low mobility material when their average energy exceeds the heterojunction energy barrier. This represents a mechanism for negative differential mobility which is similar to the Gunn effect mechanism but which occurs in real space rather than in k-space. Figure 2 shows the results of a preliminary calculation for real space electron transfer which illustrates that the Monte Carlo method predicts the process to be a real effect. We are continuing to work on many aspects of this problem. Some phases of this work will be funded by the U.S. Army Research Office.

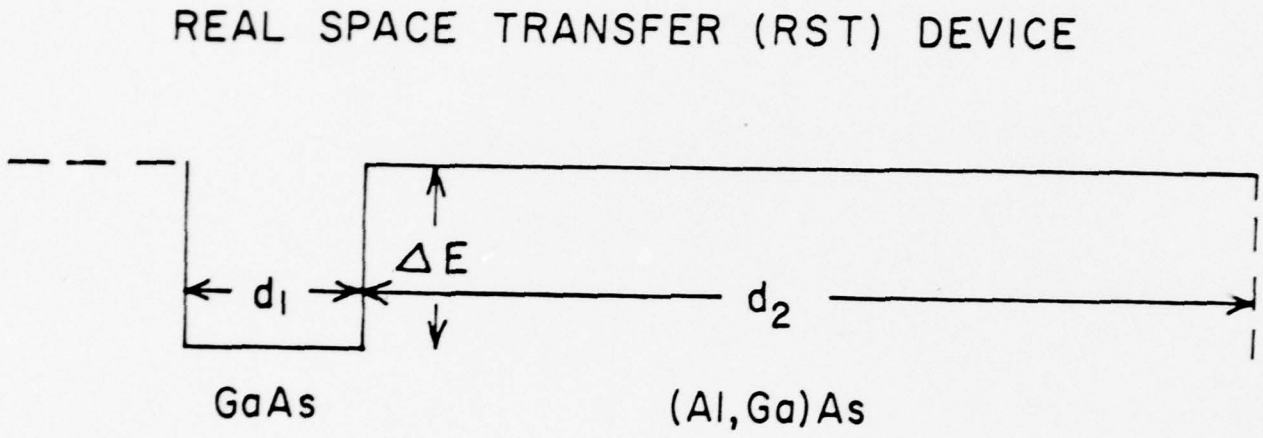

Figure 1. Schematic representation of a layered heterostructure device of GaAs/GaAlAs layers.

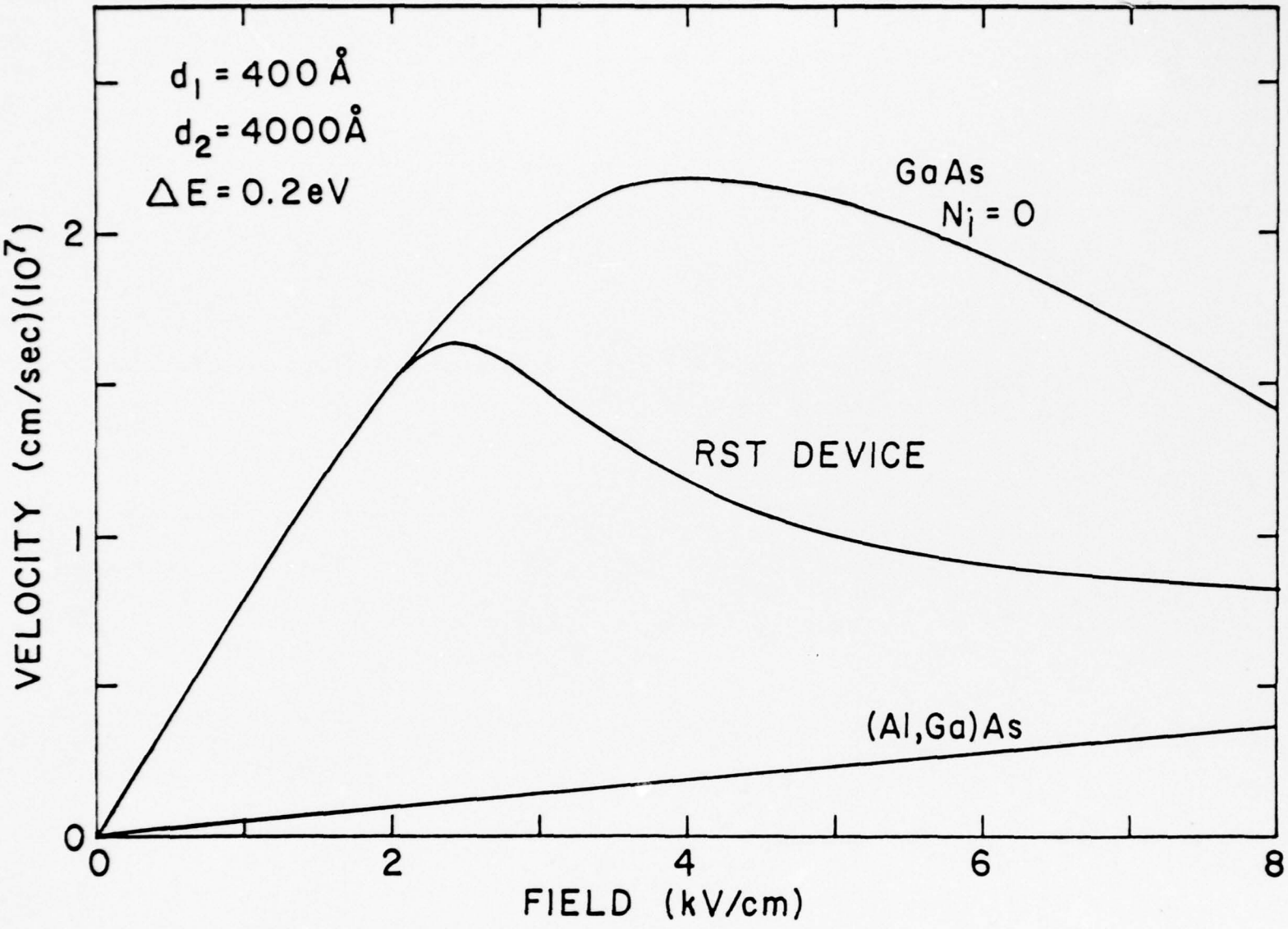

Figure 2. Velocity-field characteristics for a real space transfer device with the parameters shown compared to that for undoped GaAs.

9) Work on the two-dimensional modeling of FET devices is continuing. A general two-dimensional device model has been developed, and during the past year a considerable effort has been expended in studying the use of finite difference numerical algorithms to solve the semiconductor transport equations. We are presently not satisfied with the results achievable from this technique, primarily regarding computational accuracy and convergence. A technique has now been developed which combines the finite difference technique with finite element methods. It appears that the finite element method is now evolving as the more appropriate technique for the modeling of complicated device structures [23]. Thus, during the next year we plan to move in this direction. The long-term goal of this work is to provide a device program which will interact with the Monte Carlo program to provide a self-consistent solution for transport and terminal properties of sub-micron devices.

2.2 Publications and Presentations in 1979

A. Publications During 1978

1. M. A. Littlejohn, R. A. Sadler, T. H. Glisson, and J. R. Hauser, "Carrier Compensation and Alloy Scattering in $Ga_{1-x}In_xP_{1-y}As_y$ Grown by Liquid-Phase Epitaxy", Inst. Phys. Conf. Ser. No. 45, pp 239-247, January, 1979.

2. J. R. Hauser, T. H. Glisson, and M. A. Littlejohn, "Negative Resistance and Peak Velocity in The Central (000) Valley of III-V Semiconductors", Solid State Electronics, vol. 22, pp. 487-493, July, 1979.

3. M. A. Littlejohn, L. A. Arledge, T. H. Glisson, and J. R. Hauser, "Influence of Central Valley Effective Mass and Alloy Scattering on Transient Drift Velocity in $Ga_{1-x}In_xP_{1-y}As_y$", Electronics Letters, vol. 15, pp. 586-588, September, 1979.

B. Presentations During 1979

1. M. A. Littlejohn, J. R. Hauser, and T. H. Glisson, "III-V Compound Semiconductors For Future Electronic Devices", Invited paper presented at the Third Biennial University/Industry/Government Microelectronics Symposium, Texas Tech University, Lubbock, Texas, May 21-23, 1979. Sponsored by NSF/IEEE.

2. T. H. Glisson, J. R. Hauser, and M. A. Littlejohn, "Monte Carlo Simulations of Real Space Transfer", Paper presented at the MBE Workshop, University of Illinois, Urbana, Illinois, September 20-21, 1979. Sponsored by ONR/ARO.

3. T. H. Glisson, M. A. Littlejohn, and J. R. Hauser, "Monte Carlo Calculations of Transport in Quantum Well Structures", Paper presented at the Navy Workshop on Heterojunctions and Surfaces, Thousand Oaks, California, November, 14-15, 1979. Sponsored by ONR.

C. Paper Accepted For Publication

1. T. H. Glisson, R. A. Sadler, J. R. Hauser, and M. A. Littlejohn, "Circuit Effects in Time-of-Flight Diffusivity Measurements", accepted for publication in Solid State Electronics.

2.3 List of References

1. M. A. Littlejohn, J. R. Hauser, and T. H. Glisson, Appl. Phys. Lett. 28 458 (1977).

2. H. Morkoc, J. T. Andrews, Y. M. Houng, R. Sankaran, S. G. Bandy, and G. A. Antypas, Electron. Lett. 14 448 (1978).

3. L. F. Eastmann, private communication.

4. T. H. Glisson, J. R. Hauser, M. A. Littlejohn, and C. K. Williams, J. Electron. Mat. 7 1 (1978).

5. R. E. Nahory, M. A. Pollack, W. D. Johnston, Jr., and R. L. Barns, Appl. Phys. Lett. 33 659 (1978).

6. J. B. Restorff, Bland Houston, J. R. Burke, and R. E. Hayes, Appl. Phys. Lett. 32 189 (1978).

7. T. Nishino, Y. Yamozoe, and Y. Hamakawa, Appl. Phys. Lett. 33 861 (1978).

8. R. J. Nicholas, J. C. Portal, C. Houlbert, and P. Perrier, Appl. Phys. Lett. 34 492 (1979).

9. E. H. Perrea, E. Mendez, and C. G. Fonstad, Abstract L-4, presented at the 21st Electronic Materials Conference, Boulder, CO, June 27-29, 1979.

10. M. A. Littlejohn, R. A. Sadler, T. H. Glisson, and J. R. Hauser, Inst. Phys. Conf. Ser. 45 239 (1979).

11. R. F. Leheny, M. A. Ballman, J. C. De Winter, R. E. Nahory, and M. A. Pollack, abstract L-3 presented at the 21st Electronic Materials Conference, Boulder, CO, June 27-29, 1979.

12. G. E. Stillman, private communication.

13. R. F. C. Farrow, A. G. Cullis, A. J. Grant, and J. E. Pattison, J. Cryst. Growth 45 292 (1978).

14. A. G. Cullis and R. F. C. Farrow, Thin Solid Films 58 197 (1979).

15. R. F. C. Farrow, private communication.

16. D. L. Dexter and F. Seitz, Phys. Rev. 86 964 (1952).

17. M. A. Littlejohn, L. A. Arledge, T. H. Glisson, and J. R. Hauser, Electron. Lett. 15 586 (1979).

18. J. G. Ruch, I.E.E.E. Trans. E.D. ED-19 652 (1974).

19. J. G. Ruch and G. S. Kino, Phys. Rev. 174 921 (1968).

20. P. N. Butcher and W. Fawcett, Phys. Lett. 21 489 (1966).

21. K. Hess and B. G. Streetmann, to be published in Appl. Phys. Lett.

22. R. Dingle, H. L. Störmer, A. C. Gossard, and W. Wiegmann, Appl. Phys. Lett. 33 665 (1978).

23. NASECODE I, Numerical Simulation of Semiconductor Devices, conference held in Dublin, June 24-27, 1979.

Solid-State Electronics Vol. 22, pp. 487–493
© Pergamon Press Ltd. 1979. Printed in Great Britain
0038-1101/79/0501-0487/$02.00/0

NEGATIVE RESISTANCE AND PEAK VELOCITY IN THE CENTRAL (000) VALLEY OF III–V SEMICONDUCTORS†

J. R. HAUSER, T. H. GLISSON and M. A. LITTLEJOHN
Electrical Engineering Department, N.C. State University, Raleigh, NC 27607, U.S.A.

(*Received 7 June 1978; in revised form 30 November 1978*)

Abstract—The negative resistance in III–V materials such as GaAs at large electric fields is generally recognized as arising from the transfer of electrons from the central (000) valley to higher lying minima in the conduction band. Monte Carlo transport studies show that the negative resistance effect is still present in III–V materials when the valley spacing is increased to large values (> 0.5 eV) and even present when the higher minima are eliminated entirely from the calculations. This negative resistance arises from basic transport properties of the central valley. Studies are presented of the basic negative resistance effect in the central valley of III–V materials as well as studies of $Al_{1-x}In_xAs$ ($x \sim 0.75$) and $Ga_{1-x}In_xAs$ ($x \sim 0.6$) which are two specific materials where the negative resistance effect is due predominantly to the central valley.

1. INTRODUCTION

The negative resistance effect as first reported by Gunn[1, 2] has been observed in several of the III–V binary and ternary compounds that are direct bandgap materials. The major factors determining the negative resistance characteristic are now thought to be fairly well understood, and a good summary has recently been given by Ridley[3]. A brief summary of the conventional understanding is useful in relationship to the present work.

The negative resistance effect in GaAs has been identified with a transfer of electrons at large electric fields from the high mobility Γ or central valley to higher lying *L* or *X* minima having lower mobilities. The validity of this basic model has been verified by simple analytical calculations[3–5] as well as by more detailed Monte Carlo calculations[6–11]. The energy bands for a general III–V semiconductor are shown in Fig. 1, where $\Delta\epsilon$ is the energy separation between the central valley and the next lowest valley, which is assumed to be the *L* valley. In some materials a three band model including both the *X* and *L* minima is required to give good agreement between theory and experimental results.

In the presence of a large electric field, central valley electrons are heated by the field to large kinetic energies, and as the average kinetic energy approaches the valley separation, a large percentage of the electrons transfer to the upper valley. This transfer is enhanced by the larger effective mass of the upper valleys as compared with the central valley. Ridley has used an energy balance approach to estimate the average energy of the electrons as a function of electric field and equated this average energy to the valley separation to estimate the threshold electric field for a variety of transferred electron materials[3].

Simple considerations of the transferred electron effect lead to the conclusion that high peak velocities should be achieved in materials with (a) a large low field mobility and (b) a large energy separation between the central valley and the higher lying minima. The binary semiconductor GaAs has a relatively small valley separation on the order of 0.31 eV. The separation for InP is somewhat larger at 0.60 eV and InP is predicted to have a larger peak velocity than GaAs although the field at which the peak velocity occurs is also somewhat larger.

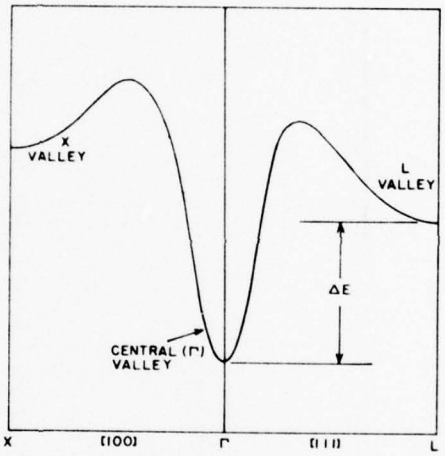

Fig. 1. Energy band diagram for general III–V direct bandgap semiconductor.

The largest valley separation in the binary III–V materials is 1.11 eV in InAs. This large valley separation, however, cannot be used in transferred electron devices (TED's) because of the low breakdown voltage of InAs due to the small bandgap of 0.36 eV. Thus, of the binary III–V materials, InP is predicted to have the largest peak velocity of the materials which are useful for TEDs.

The ternary and quaternary III–V materials provide a wider range of bandgaps and valley separations for potentially higher peak velocities than can be achieved in

†This work was supported by a research grant from the Office of Naval Research, Arlington, Virginia.

the binary materials. The quaternary $Ga_{1-x}In_xP_{1-y}As_y$ lattice matched to InP substrates has recently been predicted to have a peak velocity larger than that of either GaAs or InP[12]. The large low field mobility needed for high velocities requires low bandgap materials with small effective masses. However, too low a bandgap, as in InAs, leads to low breakdown voltages. Thus a compromise must be found between these two requirements. From breakdown voltage and device considerations, the bandgap of high velocity materials for either TEDs or FETs should probably be around 1 eV or larger.

If a minimum bandgap of around 1 eV is selected then all the III–V ternary and quaternary materials can be searched to find which material has the largest valley separation. This material turns out to be $Al_{1-x}In_xAs$ for which the energy band diagram vs composition is shown in Fig. 2. At a composition of $x = 0.75$ the energy gap is about 0.91 eV while the Γ-to-L valley separation is about 1.12 eV. Monte Carlo calculations for this composition (to be discussed in the next section) lead to a low field mobility of about 11,700 cm^2/V sec and this coupled with the large valley separation leads to an expected large peak velocity before the onset of a negative resistance effect.

Another ternary material which has a large valley separation and also has a large bandgap is $Ga_{1-x}In_xAs$ with $x \sim 0.4$–0.6. For example at $x = 0.4$ the bandgap is 0.86 eV and the valley separation is 0.72 eV. These values are not quite as good as those for the $Al_{1-x}In_xAs$ system but the technology for $Ga_{1-x}In_xAs$ is much more highly developed. The quaternary $Ga_{1-x}In_xP_{1-y}As_y$ previously reported on [12] also has a favorable bandgap and valley separation for large peak velocities.

Monte Carlo calculations on both the $Al_{1-x}In_xAs$ and $Ga_{1-x}In_xAs$ systems have not shown as large a peak velocity as initially expected. This has been found to be due to fundamental physical limitations for the peak velocity which occur within the central valley. For valley separations larger than about 0.5 eV, the peak velocity and the threshold field have been found to be determined almost entirely by the properties of the central valley. Materials with large valley separations will be referred to in this work as central valley dominated materials since such materials show a peak velocity and a negative resistance determined mainly by the central valley. The high field properties of such materials are discussed in detail in the next section.

2. CENTRAL VALLEY DOMINATED MATERIALS

The calculated velocity-field curve for $Al_{0.25}In_{0.75}As$ is shown in Fig. 3. The material parameters used in the calculations were obtained from the binary III–V parameters as discussed in previous publications[10–12] and are given in Table 1.† Included in the calculations are scattering processes due to acoustic phonons, polar optical phonons, ionized impurities ($10^{16}/cm^3$ impurity density), piezoelectric, alloy scattering processes, and equivalent and nonequivalent intervalley processes. The calculated peak velocity is about 2.7×10^7 cm/sec at a field of about 4000 V/cm. This peak value is about 35% higher than the calculated and measured values for GaAs and this verifies to some extent the discussion of the previous section as to the need for a large valley separation to achieve large peak velocities. However, the peak velocity is not as large as was expected.

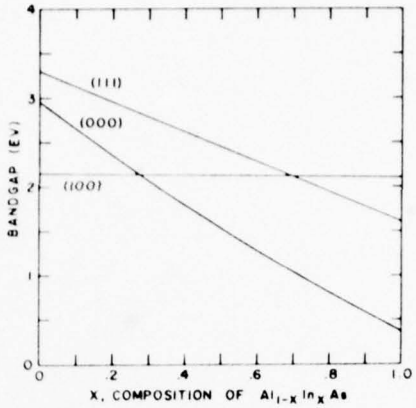

Fig. 2. Calculated energy gaps vs composition for $Al_{1-x}In_xAs$.

The numerical values shown at various points along the curve of Fig. 3 give the percentages of electrons in the L plus X minima. At the peak of the velocity curve it is seen that only 0.7% of the electrons have been transferred to the upper valleys. At 10^4 V/cm which is far into the negative resistance region only 9.2% of the electrons have been transferred to the upper valleys. These percentages which were obtained from the Monte Carlo calculations are much too low to account for the peak velocity and the negative resistance for this material. For

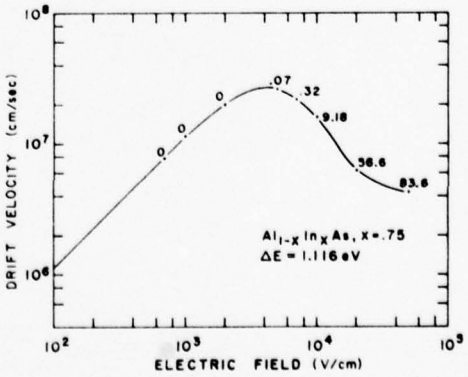

Fig. 3. Calculated velocity-field curve for $Al_{0.25}In_{0.75}As$. The values along the curve show the percentages of electrons in the upper (111 and 100) valleys.

†The possibility exists in the ternary materials of two LO phonon modes, while in the present work a single LO phonon energy is used. This has been estimated from the LO phonon energies of the binary materials and should be considered as some average phonon energy. Detailed properties of the ternary materials are not sufficiently known at present to justify the use of two LO phonons. However, the use of a single LO phonon should not detract from the main conclusions of this work.

Table 1. $Al_{0.25}In_{0.75}As$ material parameters used in the calculations

A. Bulk Material Parameters

Parameter	Value	Parameter	Value
Lattice Constant	5.959×10^{-8} cm	LO Phonon energy	0.03605 eV
Density	5.27 gm/cm^3	Sound velocity	5.11×10^5 cm/sec
Electron Affinity Diff.	1.32 eV	Optical Dielectric Constant	10.78
Piezoelectric Constant	.056 coulomb/m^2	Static Dielectric Constant	13.46

B. Valley-Dependent Material Parameters

	Conduction Band Valley		
Parameter	Γ(000)	X(100)	L(111)
Acoustic Deformation Potential (eV)	6.73	9.35	8.83
Effective Mass (m^*/m_o)	0.028	0.62	0.34
Non-Parabolicity (eV^{-1})	1.04	0.204	0.814
Energy Band Gap (eV) (relative to valence band)	0.909	2.113	2.025
Optical Deformation Potential (eV/cm)	0	0	3×10^8
Optical Phonon Energy (eV)	-	-	0.0336
Intervalley Deformation Potential (eV/cm)			
From Γ(000)	0	6.25×10^8	5×10^8
From X(100)	6.25×10^8	6.25×10^8	5×10^8
From L(111)	5×10^8	5×10^8	5×10^8
Intervalley Phonon Energy (eV)			
From Γ(000)	0	0.0253	0.0262
From X(100)	0.0253	0.0253	0.0309
From L(111)	0.0262	0.0309	0.0254
Number of Equivalent Valleys	1	3	4

example, at 10^4 V/cm a transfer of all electrons back to the central valley would increase the velocity by no more than 10% and this is much too small an effect to eliminate the negative resistance. This leads to the conclusion that the peak velocity is being controlled by the central valley in this material and is not due to electron transfer to the upper valley.

The dominance of the central valley in determining the peak velocity is shown in Fig. 4 which compares the calculated velocity-field relationship of Fig. 3 with that obtained by including only the central valley in the Monte Carlo calculations. The two calculations give very similar velocity-field relationships with the peak velocity being unchanged by the elimination of scattering to the upper valleys. A comparison of the two curves in Fig. 4 shows that transfers to the upper valleys increase the magnitude of the negative resistance beyond the peak but the upper valleys are not required for the existance of the negative resistance. Upper valley transfers are also seen to cause a larger drift velocity at very large fields (at 10^5 V/cm for example).

A similar negative resistance effect has been predicted to occur in the central valley of InSb at low temperatures (77°K)[13]. However, it does not appear to have been previously recognized that the negative resistance effect of certain ternary materials can be dominated by the central valley even at room temperature.

The dominance of the central valley is not limited to just $Al_x In_{1-x}As$ but has also been seen in other ternary materials such as $Ga_{1-x}In_xAs$ with $x \sim 0.4$–0.6. The

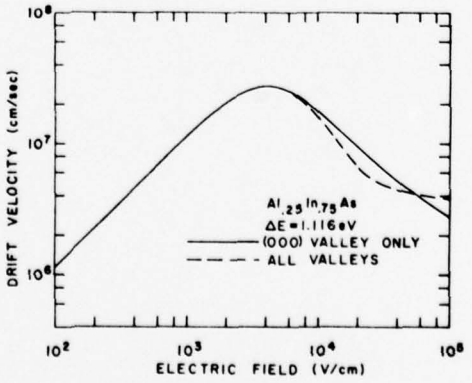

Fig. 4. Comparison of velocity-field curves for $Al_{0.25}In_{0.75}As$ using central valley only and using all valleys.

velocity field curve for this ternary with $x = 0.6$ is shown in Fig. 5. This particular material has an energy gap of 0.65 eV and a valley separation of 0.90 eV. As with $Al_{0.25}In_{0.75}As$, the presence of the upper valleys has essentially no effect on the peak velocity or threshold field for negative resistance. The upper valleys again increase the negative resistance effect and increase the high field velocity.

The two materials discussed so far have large valley separations, and this is the condition for the peak velocity and threshold field being determined by the central valley. For lower valley separations, however, such as the 0.31 eV for GaAs the question arises as to how important is the intervalley transfer of electrons in determining the peak velocity. Calculations for GaAs have shown that without the L and X valleys present the velocity would peak at about 2.5×10^7 cm/sec as opposed to the value of about 2.0×10^7 cm/sec including the upper valleys. Thus the transfer of carriers to the upper valleys reduces the peak velocity in GaAs by about 20%.

The central valley dominated materials such as shown in Fig. 4 are predicted by the Monte Carlo calculations to have a large peak-to-valley ratio for the velocity-field curve. The peak-to-valley ratio in Fig. 4 ranges from about 4 to 7 for peak fields from 20 to 100 kV. For GaAs with a smaller valley spacing, the peak-to-valley ratio is at most about 2.5 by both experimental measurement[14] and theoretical calculations[15]. This large peak-to-valley ratio for the central valley dominated semiconductors may be especially useful in certain device applications.

The preceding discussion has demonstrated that when the valley spacing becomes large the peak velocity and threshold field are no longer determined by electron transfer from the central valley to higher lying minima. The peak velocity is rather determined by the fundamental transport properties of the central valley. In order to understand these central valley limitations a study has been made of the high field properties of model semiconductors with only a central valley. These studies are discussed in detail in the next section.

3. TRANSPORT IN CENTRAL VALLEY ONLY

This section considers a semiconductor in which the spacing between the central valley [$\Gamma(000)$ valley] and higher lying minima (either X or L valley) is so large that only the central valley must be considered in the transport. In all of the III–V ternary and quaternary materials the spacing can never be made so large that it has no effect on the transport process. However, as the previous section illustrates, the spacing can be so large that intervalley transfers have a negligible effect on the peak velocity and threshold field for certain materials. A study of transport in only the central valley can thus lead to an understanding of the physical processes leading to a peak velocity and negative resistance effect in these materials as well as provide an upper limit to the peak velocity for other materials. Since the $Al_{0.25}In_{0.75}As$ comes closest of all the ternary III–V materials to being dominated by the central valley, the parameters for the calculations presented in this section using only the central valley are selected as those of this material, and are listed in Table 1.

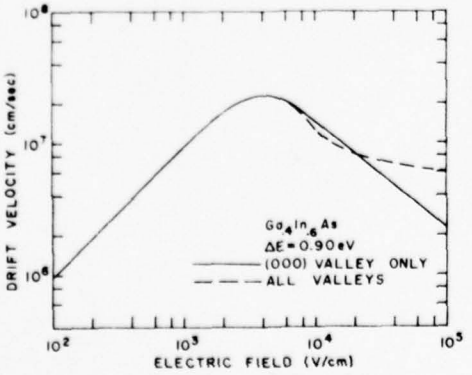

Fig. 5. Velocity-field curves for $Ga_{0.4}In_{0.6}As$.

The negative resistance and peak velocity in the central valley have been found to be due to the fundamental properties of the nonparabolic bands of the central valley as first discussed by Persky and Bartelink[13]. The negative resistance occurs when the nonparabolic bands are considered with only the dominant scattering process of polar optical scattering. This is seen in Fig. 6 which compares the velocity-field curve for only polar optical scattering with the corresponding curve including all scattering processes. The general shape of the curves is seen to be determined by polar optical scattering with the other scattering processes simply reducing the velocity by almost a constant factor at all field values. This dominance of polar optical scattering is to be expected since it is the major energy loss process.

The presence of a negative resistance in Monte Carlo calculations when only polar optical scattering is considered is at first very surprising. This differs from previous studies where it has been shown that only polar optical scattering leads to an energy runaway condition at large electric fields[16–18]. As shown below the difference between these earlier studies and the present study arises from the description of the energy bands. The studies referenced above considered parabolic energy bands while the present work has considered a non-parabolic band described by

$$\frac{\hbar^2 k^2}{2m^*} = \gamma(\epsilon) = \epsilon(1 + \alpha\epsilon), \tag{1}$$

where m^* is the effective mass at $\epsilon = 0$ and α is the first order non-parabolicity factor[19]. With parabolic bands one gets energy runaway and with non-parabolic bands one does not.

The basic physics of high field transport can be described analytically by energy and momentum balance equations of [3]

$$m_e^* \frac{dv}{dt} = qE - \frac{m_e^* v}{\tau_m} = 0, \tag{2}$$

$$\frac{d\epsilon}{dt} = qEv - \frac{\epsilon - \epsilon_T}{\tau_\epsilon} = 0, \tag{3}$$

where E is the electric field, m_e^* the energy dependent effective mass, ϵ_T the thermal energy, τ_m the momentum relaxation time and τ_e the energy relaxation time. These can be combined and solutions obtained for E and v as

$$E = \left(\frac{m_e^*(\epsilon - \epsilon_T)}{q^2 \tau_m \tau_e}\right)^{1/2}, \tag{4}$$

$$v = \left(\frac{\epsilon - \epsilon_T}{m_e^*}\frac{\tau_m}{\tau_e}\right)^{1/2}. \tag{5}$$

If a model is available for τ_m and τ_e as functions of energy, these equations express E and v as functions of average electron energy. By solving these for various values of energy, v as a function of E can be obtained.

For polar optical scattering only and at large energies ($\epsilon \gg \hbar\omega_0$) the relaxation rates can be approximated as[3].

$$\frac{1}{\tau_m} = \frac{q^2(2m^*)^{1/2}\hbar\omega_0}{8\pi\hbar^2}\left(\frac{1}{\epsilon_\infty} - \frac{1}{\epsilon_0}\right)\frac{1}{\gamma(\epsilon)^{1/2}}\frac{d\gamma(\epsilon)}{d\epsilon}[2n(\omega_0) + 1],$$

$$\frac{\epsilon - \epsilon_T}{\tau_e} = \frac{q^2(2m^*)^{1/2}(\hbar\omega_0)^2}{8\pi\hbar^2}\left(\frac{1}{\epsilon_\infty} - \frac{1}{\epsilon_0}\right)\frac{1}{\gamma(\epsilon)^{1/2}}\frac{d\gamma}{d\epsilon} \tag{6}$$

$$\times \ln\left[4\gamma(\epsilon)\left(\hbar\omega_0\frac{d\gamma(\epsilon)}{d\epsilon}\right)^{-1}\right], \tag{7}$$

where $\hbar\omega_0$ is the optical phonon energy and $n(\omega_0)$ is the Bose–Einstein factor. More detailed and complete treatments of the relaxation rates can be found in Refs. [20, 21]. However, the present simple expressions appear to contain all the information needed to understand the central valley negative resistance. The energy dependent effective mass can also be approximated as

$$m_e^* = m^*\left(\frac{d\gamma(\epsilon)}{d\epsilon}\right)^2\left(\frac{\epsilon}{\gamma(\epsilon)}\right). \tag{8}$$

In a parabolic band ($\gamma = \epsilon$, $(d\gamma/d\epsilon) = 1$) both the rates of momentum loss and energy loss decrease with energy. This makes it impossible to achieve steady state above a certain energy. For a non-parabolic band as described by eqn (1), τ_m^{-1} approaches a constant at large energies while $(\epsilon - \epsilon_T)/\tau_e$ increases slowly with energy as $\ln(2\epsilon/\hbar\omega_0)$. In this type of energy band a steady state solution can be found at any energy.

The analytical model as expressed by eqns (4)–(8) has been solved for the parameters given in Table 1 and for the energy band of eqn (1). The results for velocity as a function of field are plotted as points in Fig. 6. Excellent agreement is seen between the results of the analytical model and the Monte Carlo calculations. This supports the accuracy of the Monte Carlo results and demonstrates that negative resistance is a feature of the central valley when non-parabolic energy bands are considered.

Two basic questions can still be raised with respect to the results reported here. First, the energy band is in reality more complicated than the form expressed in eqn (1). This equation approaches a linear E vs k relationship at large energies while real bands have a region of negative effective mass at large energies. In such an energy band, the electron energy for a given field will be

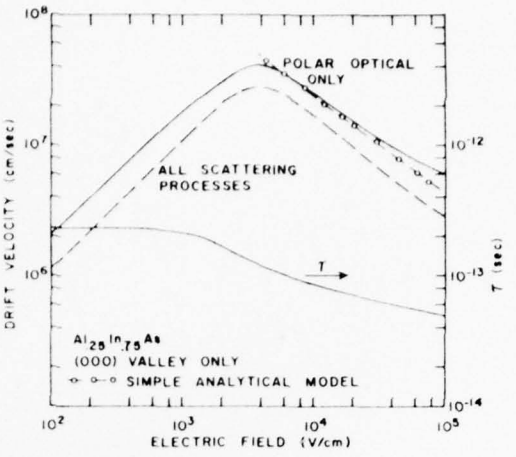

Fig. 6. Velocity-field curve for central valley with just polar optical scattering.

even less than that given by a band described by eqn (1). Thus if energy runaway does not occur with a band described by eqn (1), it will not occur in a band where energy increases more slowly with k. Also the negative effective mass region of a band can by itself lead to a negative resistance at high fields. Thus a more accurate description of the nonparabolic band should enhance the negative resistance calculated in the present work.

A second question arises as to the neglect of p-state mixing in the model for the relaxation rates of eqns (6) and (7)[7]. In order to compare the Monte Carlo and analytical results, the Monte Carlo results reported in Fig. 6 did not include p-state mixing in the calculations. A comparison of the Monte Carlo results both including and neglecting p-state mixing is shown in Fig. 7. As can be seen there is little difference in the overall results. The velocity including p-state mixing is just slightly larger than that neglecting p-state mixing. Thus the existence of the negative resistance region is not sensitive to the exact model used for polar optical scattering.

A simple interpretation of the positive and negative resistance regions can be obtained from the momentum and energy balance equations. The energy balance equa-

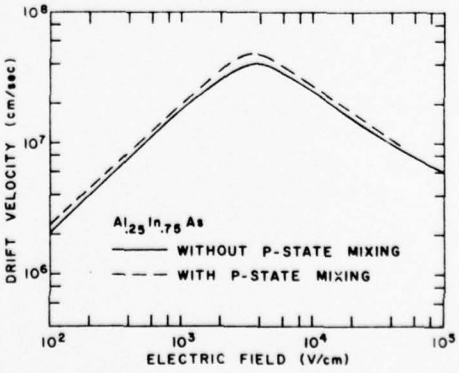

Fig. 7. Comparison of calculated velocity field curves including and not including p-state mixing in the scattering rates.

tion can be written in a slightly different form from eqn (3) when only polar optical scattering is considered,

$$qEv = \frac{\Delta\epsilon(P_e - P_a)}{\tau_0}, \tag{9}$$

where $\Delta\epsilon = \hbar\omega_0$, P_e is the probability of phonon emission, P_a is the probability of phonon absorption, τ_0 is the mean time between scattering and $\epsilon \gg \hbar\omega_0$. It should be noted that τ_0 is not exactly the same as τ_ϵ used in eqn (3). At large energies

$$P_e - P_a \to \left(\frac{e^x - 1}{e^x + 1}\right) = \tanh(x/2), \tag{10}$$

where $x = \hbar\omega_0/kT$.

From the momentum and energy relaxation times, the velocity can then be expressed as

$$v = \frac{q\tau_m}{m_x^*} E, \tag{11}$$

$$v = \frac{\hbar\omega_0 \tanh(\hbar\omega_0/2kT)}{q\tau_0} \frac{1}{E}, \tag{12}$$

where eqn (12) is only valid at large energies. At low fields and low particle energies where $m_x^* = m^*$ and τ_m are constant, eqn (11) predicts a linearly increasing velocity with field. At large fields if τ_0 were constant eqn (12) predicts a decreasing velocity with increasing field. The Monte Carlo results and eqn (7) actually show that τ_0^{-1} increases with particle energy as $\ln(\epsilon)$, and ϵ in turn increases as E^2 at large fields. These combine to make τ_0^{-1} increase as $\ln(E)$. This is a weak dependence and does not compensate for the E^{-1} dependence of eqn (12). Equation (11) is also satisfied at large fields because m_x^* increases with energy and field.

Equations (11) and (12) can be used to provide an upper limit on the velocity which can be achieved in a semiconductor. By equating the limiting expressions of eqns (11) and (12) and taking $\tau_m = \tau_0$† and solving for $qE\tau_m/m^*$, one obtains

$$v_p \leq v_{max} = \left[\frac{\hbar\omega_0}{m^*} \tanh(\hbar\omega_0/2kT)\right]^{1/2}. \tag{13}$$

Values of v_{max} for several binary and compound materials are shown in Fig. 8. Also shown for several materials are the peak velocity values that result from Monte Carlo calculations including all bands and all scattering processes. For the binary materials GaAs, InP and InAs the Monte Carlo results give peak velocities that are about 82–90% of the values predicted by eqn (13). For the two ternary and one quaternary materials shown, the Monte Carlo results differ from eqn (13) by large amounts. The lower Monte Carlo result for the ternary and quaternary materials is due to the presence of alloy scattering in these materials which is not present in the binary materials. If alloy scattering had not been included all of the Monte Carlo results would have been around 80–90% of the limiting value given by eqn (13).

Monte Carlo results are not shown for InSb and GaSb. The band-gap of InSb is too low for this material to be used near the peak velocity. For GaSb the presence of the L minima at only 0.09 eV above the Γ minima causes the negative resistance effect not to occur in this material. The data in Fig. 8 indicates that there is a general trend toward larger peak velocities as the bandgap of the semiconductor decreases.

The fundamental roles of polar optical scattering and band nonparabolicity in the central valley combine to determine the peak velocity which can be achieved. Figure 9 shows the velocity field curves for the central valley only of $Al_{0.25}In_{0.75}As$ with different α values, where the theoretical value of

$$\alpha = \frac{1}{\epsilon_g}\left(1 - \frac{m^*}{m_0}\right)^2, \tag{14}$$

gives 1.04 eV^{-1} for $Al_{0.25}In_{0.75}As$. This corresponds to one of the curves in Fig. 9. Also shown are velocity field curves for α values an order of magnitude smaller and an order of magnitude larger than the theoretical value. For values of α less than 0.104 the calculated values are close to the 0.104 curve of Fig. 9. At the theoretical value of α the nonparabolicity is seen to reduce the low field mobility by about 37%, to reduce the peak velocity slightly, and to increase the threshold field from around 3 kV/cm to around 4 kV/cm. A very large nonparabolicity ($\alpha = 10.4$ eV^{-1}), which fortunately does not occur in the III–V materials, is seen to drastically reduce the low field mobility and the peak velocity. The nonparabolicity will be most important in materials with narrow bandgaps and large valley spacings, since α is large for such materials and the carriers become heated to large energies before intervalley transfer occurs.

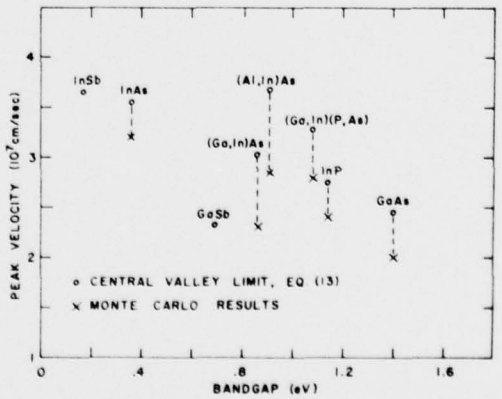

Fig. 8. Calculated upper limits to peak velocity considering central valley only.

†τ_m and τ_0 are only equal for special scattering processes such as isotropic scattering. They are not exactly equal for polar optical scattering. However, the limiting expression obtained in this manner has been found to provide a good upper limit to the peak velocity for a variety of semiconductors.

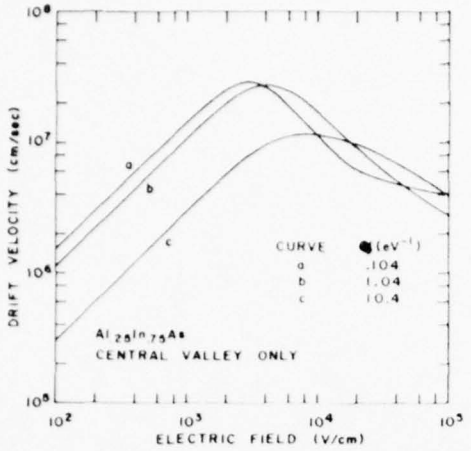

Fig. 9. Velocity field curves for $Al_{0.25}In_{0.75}As$ with different nonparabolicity factors. The theoretical value is $\alpha = 1.04\,eV^{-1}$.

4. SUMMARY AND CONCLUSIONS

The presently accepted theory of negative resistance effects in III–V semiconductors attributes the effect to the transfer of electrons from a high mobility central (Γ) valley to lower mobility, higher lying energy valleys (L or X). The present work has shown that in materials with a large valley spacing the negative resistance becomes dominated by the central valley. Monte Carlo calculations have shown that the presence of the upper valleys is not required for a negative resistance effect but that polar optical scattering acting in a nonparabolic central valley alone gives rise to a peak velocity and negative resistance effect. For materials with valley spacings of 0.5 eV or larger the peak velocity and threshold field has been found to be determined almost entirely by the central valley negative resistance effect. Transfers to the upper valleys influence mainly the magnitude of the negative resistance and the carrier velocity near the valley minimum of the velocity field curve.

Materials which have large valley spacings and are dominated by the central valley have large peak-to-valley velocity ratios as predicted by Monte Carlo calculations. The ternary materials $Al_{1-x}In_xAs$ ($x \sim 0.75$), $Ga_{1-x}In_xAs$ ($x \sim 0.5$) and the quaternary $Ga_{1-x}In_xP_{1-y}As_y$ ($x \sim 0.75$, $y \sim 0.4$) are typical of central valley-dominated materials. The largest peak velocities which have so far been calculated by the Monte Carlo technique have been found in these materials.

Acknowledgements—The assistance of K. Williams and J. Shade in the calculations reported in this work are gratefully acknowledged.

REFERENCES

1. J. B. Gunn, *Solid St. Commun.* **1**, 88 (1963).
2. J. B. Gunn, *IBM J. Res. Dev.* **8**, 141 (1964).
3. B. K. Ridley, *J. Appl. Phys.* **48**, 754 (1977).
4. B. K. Ridley and T. B. Watkins, *Proc. Phys. Soc. (Lond.)* **78**, 293 (1961).
5. D. E. McCumber and A. G. Chynoweth, *IEEE Trans. on Electron. Dev.* **ED-14**, 4 (1966).
6. T. Kurosawa, *Proc. Int. Conf. Semicond. Kyoto, J. Phys. Soc. Jpn. Suppl.* **21**, 424 (1966).
7. W. Fawcett, A. D. Boardman and S. Swain, *J. Phys. Chem. Solids* **31**, 1963 (1970).
8. J. G. Ruch and W. Fawcett, *J. Appl. Phys.* **41**, 3843 (1970).
9. W. Fawcett and D. C. Herbert, *J. Phys. Chem.* **7**, 1641 (1974).
10. M. A. Littlejohn, J. R. Hauser and T. H. Glisson, *Appl. Phys. Lett.* **26**, 625 (1975).
11. J. R. Hauser, M. A. Littlejohn and T. H. Glisson, *Appl. Phys. Lett.* **28**, 458 (1976).
12. M. A. Littlejohn, J. R. Hauser and T. H. Glisson, *Appl. Phys. Lett.* **30**, 242 (1977).
13. G. Persky and D. J. Bartelink, *IBM Journal* **13**, 607 (1969).
14. P. A. Houston and A. G. R. Evans, *Solid-St. Electron.* **20**, 197 (1977).
15. M. A. Littlejohn, J. R. Hauser and T. H. Glisson, *J. Appl. Phys.* **48**, 4587 (1977).
16. E. M. Conwell, *High Field Transport in Semiconductors*, pp. 199–201. Academic Press, New York (1967).
17. H. Frohlich and B. V. Paranjape, *Proc. Phys. Soc. (London)* **1369**, 21 (1956).
18. R. Stratton, *Proc. Roy. Soc.* **A246**, 406 (1958).
19. E. M. Conwell and M. O. Vassell, *Phys. Rev.* **166**, 797 (1968).
20. D. Matz, *Phys. Rev.* **168**, 843 (1967).
21. R. C. Curby and D. K. Ferry, *Phys. Rev.* **B3**, 3379 (1971).

Circuit Effects in Time-of-Flight Diffusivity Measurements

T. H. Glisson, R. A. Sadler, J. R. Hauser, and M. A. Littlejohn

Department of Electrical Engineering
North Carolina State University, Raleigh, NC 27650

Abstract

A monte carlo procedure is used to examine certain effects that interfere with the determination of the diffusivity D from current rise and fall times in a time-of-flight experiment. It is found that electron bombardment time, sample capacitance, contact resistance, and oscilloscope rise time can cause considerable error in the measurement of D, especially near the threshold electric field. It is shown that a reasonable accounting for these effects can explain much of the difference between experimentally-and theoretically-determined D-E characteristics for GaAs.

This work was supported by the Office of Naval Research.

Introduction

Extensive measurements of the transport properties of electrons in GaAs were reported by Ruch and Kino in 1968 [1]. It has proved difficult to bring monte-carlo calculations of the diffusivity versus field (D-E) characteristic into agreement with the experimental D-E characteristic in [1] without sacrificing some agreement elsewhere, e.g., with velocity-field (v-E) or mobility-temperature (μ-T) measurements. This state of affairs is illustrated in Fig. 1, where three calculated (monte-carlo) D-E characteristics are superimposed on the experimental (RK) D-E characteristic from [1]. Curve A, calculated by Abe, et al [2], is in good agreement with the experimental data for $E \gtrsim 2$kV/cm, but leads (through the Einstein relation) to a low-field mobility that is about twice the accepted value. Curve L was calculated by the present authors using the model proposed by Littlejohn, et al [3]. That model yields calculated v-E and μ-T characteristics that are in good agreement with experimental data, yet yields a D-E characteristic (curve L in Fig. 1) that is quite different from that measured by Ruch and Kino. Curve PR in Fig. 1 was calculated by Pozela and Reklaitis [4] using a model that is only slightly different from the one described in [3]. The present authors have been unable to reproduce this result, and cannot attribute the great differences between curves L and PR to the slight difference between the models described in [3] and [4].

The experimental (RK) characteristic itself is questionable in two regards. First, it rises sharply in the ohmic region ($0 < E < 2$kV), whereas D should be nearly independent of E there because of the Einstein relation. Second, the RK characteristic appears (when extrapolated)

to approach ≈100 - 150 cm^2/s at large fields, whereas experimental data indicate that D does not exceed 20 cm^2/s at E = 50 kV/cm [5].

In Ruch and Kino's paper [1] the experimental D-E characteristic was compared to one attributed to Butcher and Fawcett [6]* and it was suggested that the considerable differences were due in part to "inter-valley diffusion". However, it is hard to see how this effect could have been excluded from the monte-carlo calculation described in [6], since a two-valley model was used.

In this paper we suggest that some of the differences between the experimental and calculated D-E characteristics might be due to seemingly negligible circuit effects that interfere with the measurement scheme described in [1]. These circuit effects include the sample capacitance, contact resistance, imperfect matching, oscilloscope rise time, and the like.

Theory of Diffusivity Measurement

In the time-of-flight experiment, carriers are injected at the cathode and drift under the applied field to the anode. Diffusion causes the spatial distribution of carriers to spread during the drift. Ruch and Kino assumed (see Appendix C of [1]) the spatial distribution of carriers to be gaussian with mean $\bar{x} = vt$ and variance $\sigma_x^2 = 2Dt$, where v and D are the drift velocity and diffusivity, respectively. Thus the carriers reach the anode at times near ℓ/v, where ℓ is the sample thickness. At that time $\sigma_x = \sqrt{2D\ell/v}$, and the current falls from 95% to 5% of its peak value in a time given by $\tau_F = 3.28\ \sigma_x/v$. Thus the diffusivity can be obtained

*Actually, no D-E data are given in [6]. The D-E data attributed in [1] to [6] appear to have been obtained from the v-E data in [6] via the Einstein relation.

from a measurement of the 95%-5% current fall time through

$$D = \frac{\tau_F^2 v^3}{21.6\ell} \tag{1}$$

where v is obtained from the sample thickness and transit time (the time at which the current has fallen to 50% of its peak value).

The more elaborate development given in Appendix C of [1] leads to

$$D = \frac{(\tau_F^2 - \tau_R^2) v^3}{21.6\ell} \tag{2}$$

where τ_R is the 5%-95% current pulse rise time and v is obtained from the sample thickness and the elapsed time between the 50% rise and fall times. However, it is not clear that diffusion effects have anything at all to do with the shape of the leading edge of the current pulse; the inclusion of τ_R in Eq. (2) is perhaps best regarded as an attempt to compensate for circuit effects and the finite time for which the sample is bombarded (to inject carriers). Ruch and Kino state correctly that Eq. (2) compensates exactly for circuit effects if the rates of current rise and fall and the circuit impulse response are gaussian, but the assumption of a gaussian circuit impulse response is hard to justify. An exponential circuit impulse response seems more likely, in which case Eq. (2) can give wrong values for D.

Circuit Model and Results

The experimental apparatus and set-up used by Ruch and Kino are described in [1], where rise (and fall) times of "as much as 0.2 ns" were attributed to sample and support capacitance, contact resistance, and the like. The oscilloscope rise time was 0.06 ns, and the sample was bombarded by electrons (to inject carriers) for times on the order of 0.1 ns. The electron-hole pairs were created within 3 μm of the

cathode. These effects and others (such as space charge) contribute to τ_R and τ_F in Eq. (2), perhaps as much as or more than diffusion, and may distort the value of D thus obtained.

A first-order accounting for circuit effects can be made by superimposing the responses of a single-pole (R-C) circuit to a number of rectangular current pulses, each of which represents the contribution of a single electron to the total current through (or voltage across) the sample. This is illustrated in Fig. 2, where an individual current source is described by

$$i_n(t) = \frac{k(\ell - x_n)}{\Delta t_n} [u(t-t_n) - u(t-t_n - \Delta t_n)]. \tag{3}$$

(In Eq. (3), k is a dimensioned constant that accounts for charge density, sample cross-sectional area, and electronic charge.) In the calculations to be described here, x_n is randomly selected from the interval [0,3μm] (to account for penetration of the bombarding electrons), t_n is randomly selected from the interval [0,0.1 ns] (to account for the time for which the sample is bombarded), and Δt_n is selected from the density

$$f(\ell - x_n, \Delta t_n) = \frac{\ell - x_n}{\sqrt{4\pi D \Delta t_n^3}} e^{-(\ell - x_n - v\Delta t_n)^2/(4D\Delta t_n)} \tag{4}$$

which is the density of the time to absorption (Δt_n) for Brownian particles released (at t=0) a distance $\ell - x_n$ to the left of an absorbing boundary (the anode) [7]. In the Ruch-Kino experiment and in the calculations here, the sample thickness ℓ = 0.03 cm.

Our procedure was as follows: (1) The field dependence of v and D in Eq. (4) was obtained by a monte-carlo calculation from the model described in [3]. This is equivalent to assuming that curve L in Fig. 1 is the "correct" one that would be observed in the absence of interfering effects; (2) For each field (1kV/cm $\leq$ E $\leq$ 12 kV/cm), one thousand values

each for x_n, t_n, and Δt_n were selected as described above; (3): The circuit response (simulated pulse) was constructed from

$$r(t) = \sum_{n=1}^{1000} \frac{k(\ell - x_n)}{\Delta t_n} [g(t-t_n) - g(t-t_n-\Delta t_n)] \tag{5}$$

where

$$g(t) = [1-e^{-t/\tau_c}]u(t) \tag{6}$$

is the step response of the circuit for time constant τ_c; (4): The 5%-95% rise time τ_R, 95%-5% fall time τ_F, and 50%-50% pulse duration τ_T (transit time) of the simulated pulse r(t) were determined; and (5): The drift velocity v was calculated as $v = \ell/\tau_T$ and the diffusivity was then calculated using Eq. (2).

The calculation just described was performed for several values of the circuit time constant τ_c. The best agreement between the simulated and experimental D-E characteristic was obtained for $\tau_c = 0.25$ ns. The results are shown in Fig. 3. The dashed curve is the experimental data from [1], and the solid circles are the diffusivities calculated from Eq. (2) as described above. Curve L is repeated from Fig. 1, and shows the specified diffusivities used in Eq. (4) for the random selection of the individual carrier transit times. Curve L and the v-E data used in Eq. (4) were calculated by the authors using the model described in [3] with impurity concentration $N = 10^{14} cm^{-3}$. This impurity concentration is reasonably consistent with the sample resistivities given in [1].

The observed D-E characteristic in Fig. 3 is in good qualitative agreement with the experimental data, but is displaced toward higher fields. This displacement is due to the fact that the model used leads

to a v-E characteristic that is displaced to the right relative to that measured and used to calculate D in [1]. The v-E characteristic measured in [1] is in much better agreement with that in [6] than that in [3], so the calculations described above were repeated using the theoretical v-E and D-E data attributed in [1] to Butcher and Fawcett [6]. The best fit circuit time constant was τ_c = 0.22 ns, and the results are shown in Fig. 4. The simulated D-E characteristic is closer to the experimental characteristic than in Fig. 3, mainly because the peaks more nearly coincide.

Conclusions

The circuit time constants $\tau_c \simeq$ 0.25 ns and 0.22 ns used to obtain the results just described are reasonably consistent with the estimates given in [1] (0.2 ns for sample & supports, 0.06 ns for the oscilloscope), and lead to observed (measured) diffusivities that are greatly inflated near their peak value. The term τ_R^2 in Eq. (2) does not compensate for the circuit effects, although it was found to almost compensate for the effects of the 0.1 ns bombardment time. It was first thought that the circuit effects would also disturb the transit time measurement, and thus the measurement of v, because the leading and trailing pulse edges have different slopes and would suffer different delays; this was not found to be a problem for the time constants considered here. The calculated drift velocity was always within a few percent of that specified in Eq. (4) for the selection process.

The impact of the circuit effects on the measurement of D is further illustrated by Fig. 5. Here the specified v and D were calculated at E = 4kV/cm using the model in [3] with $N = 10^{14} cm^{-3}$. Thus the "true" diffusivity is 300 cm^2/s, as was observed for a circuit time constant of zero. The simulated diffusivity remains close to the actual (specified) diffusivity for $\tau_c < 0.05$ ns, and rises sharply for $\tau_c > 0.15$ ns. At $\tau_c = 0.25$ ns, the simulated diffusivity is about 900 cm^2/s, and corresponds to the peak value of the observed D in Fig. 3.

Equation (2) can give good results if the external circuit effects are small compared to the effects of diffusion. In terms of the model used here, this requires that the circuit time constant τ_c be small compared to the fall time τ_F due to diffusion alone at all fields of interest. The fall time τ_F is on the order of $2\sigma_x(\tau_T)/v = 2\sqrt{2D\ell/v^3}$, and is smallest near threshold. Based on this simple argument, it appears Eq. (2) is useable provided

$$\tau_c << \sqrt{8D\ell/v^3} \quad . \tag{7}$$

For GaAs and E = 4kV/cm we find $\sqrt{8D\ell/v^3} \simeq 0.1$ ns. As expected, this value is also roughly that at which the curve in Fig. 5 begins to turn upward.

If the inequality in Eq. (7) is not satisfied, circuit effects must somehow be accounted for. If the circuit effects can be modelled, a procedure like the one described in the previous section can be used to construct curves like the one in Fig. 5 for various "actual" values for D. These curves could then be used to correct the results obtained from Eq. (2).

References

1. J. G. Ruch and G. S. Kino, Phys. Rev. 174, 921 (1968).

2. M. Abe., S. Yanagisawa, O. Wada and H. Takanashi, Appl. Phys. Lett. 25, 674 (1974).

3. M. A. Littlejohn, J. R. Hauser and T. H. Glisson, J. Appl. Phys. 48, 4587 (1977).

4. J. Pozela and A. Reklaitis, Solid St. Commun. 27, 1073 (1978).

5. A. Castelain, R. Perichon, E. Constant and A. Le Borgne, Appl. Phys. Lett. 25, 721 (1974).

6. P. N. Butcher and W. Fawcett, Phys. Lett. 21, 489 (1966).

7. W. Feller, An Introduction to Probability Theory and Its Applications, Vol. I, p. 326. Wiley, New York (1957).

Figure Captions

Fig. 1. Diffusivity versus applied electric field for electrons in GaAs. RK: experimental data from [1]; A: Monte-carlo calculation from [2]; PR: Monte-carlo calculation from [4]; L: Monte-carlo calculation by the present authors using the model described in [3].

Fig. 2. Circuit model used in the calculation of the simulated diffusivity. (see text).

Fig. 3. Simulated diffusivity versus field when the "actual" (specified in Eq. 4) D-E and v-E values are obtained from the model in [3] (with $N = 10^{14}\ cm^{-3}$). $\tau_c = 0.25$ ns.

Fig. 4. Simulated diffusivity versus field when the "actual" D-E and v-E are obtained from [1], attributed there to [6]. $\tau_c = 0.22$ ns.

Fig. 5. Simulated peak diffusivity versus circuit time constant. The specified diffusivity (300 cm^2/s) and drift velocity in Eq. (4) were calculated from the model in [3].

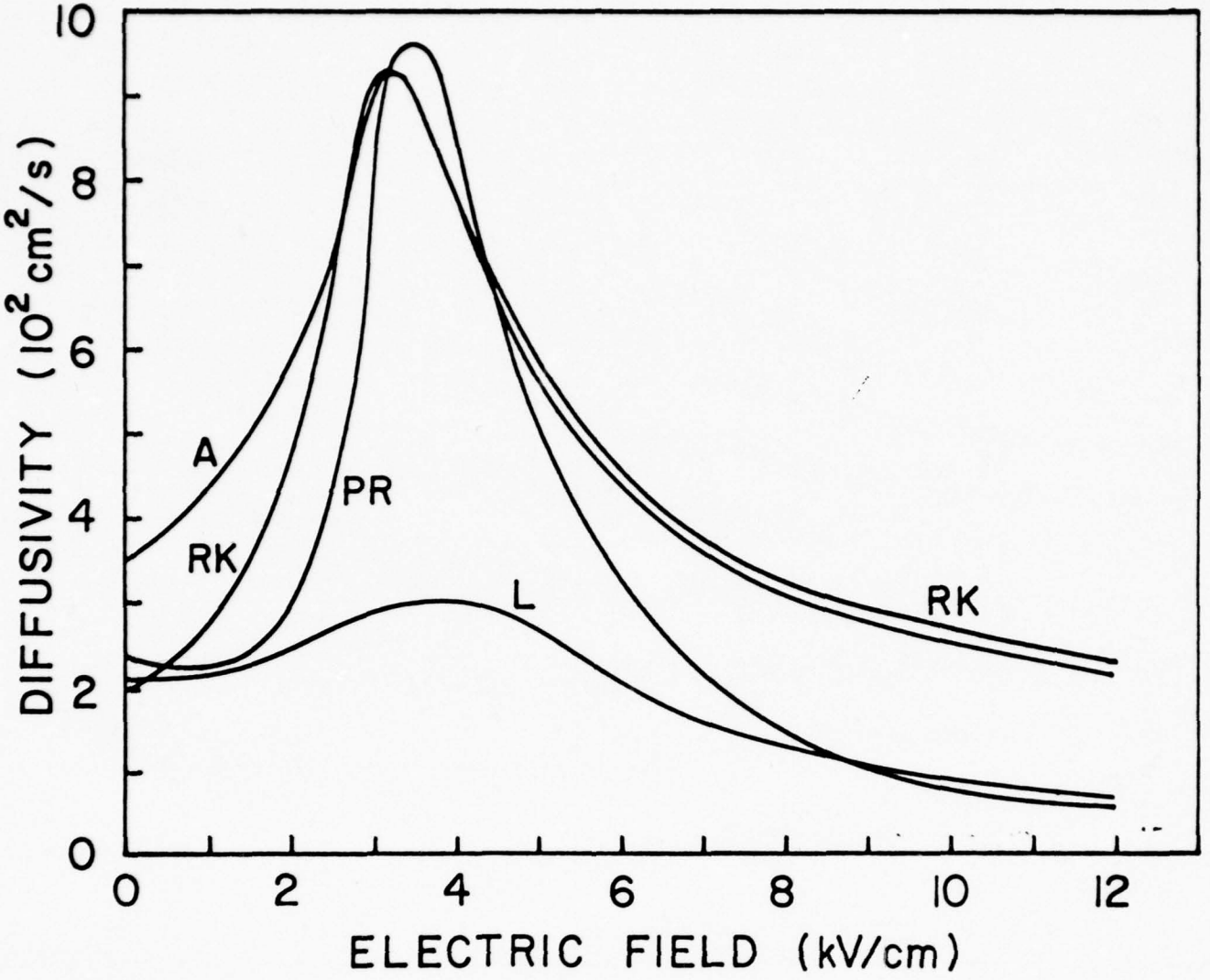
DIFFUSIVITY (10^2 cm^2/s)
ELECTRIC FIELD (kV/cm)
0
2
4
6
8
10
12
A
RK
PR
L
RK

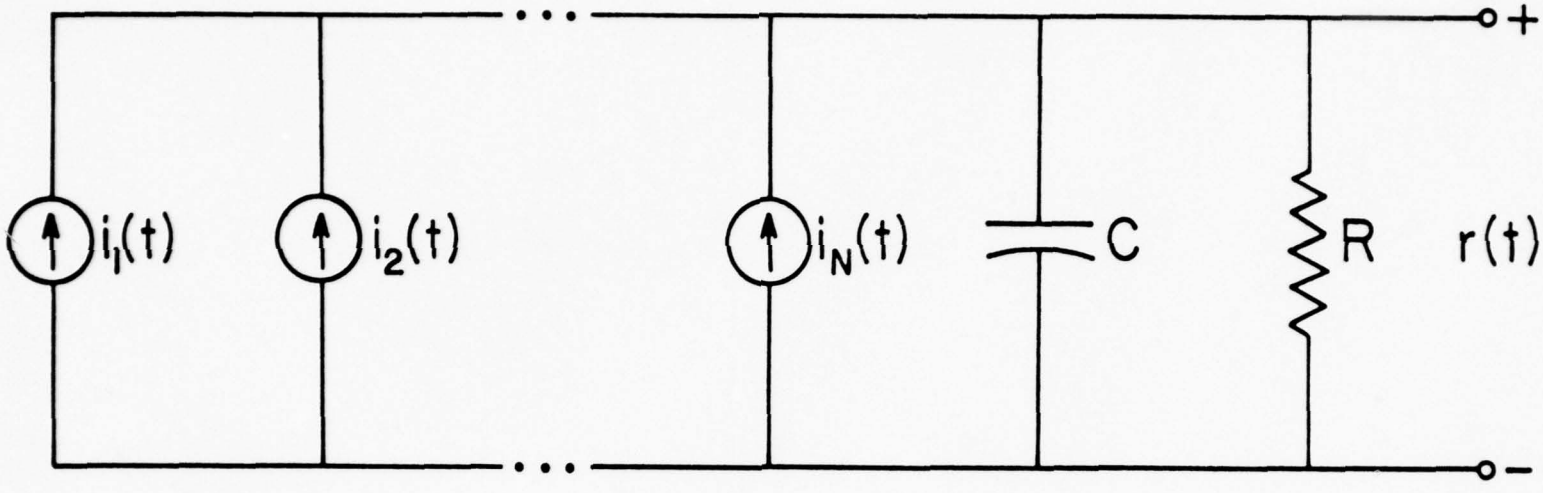
+
$i_1(t)$
$i_2(t)$
$i_N(t)$
C
R
r(t)
-

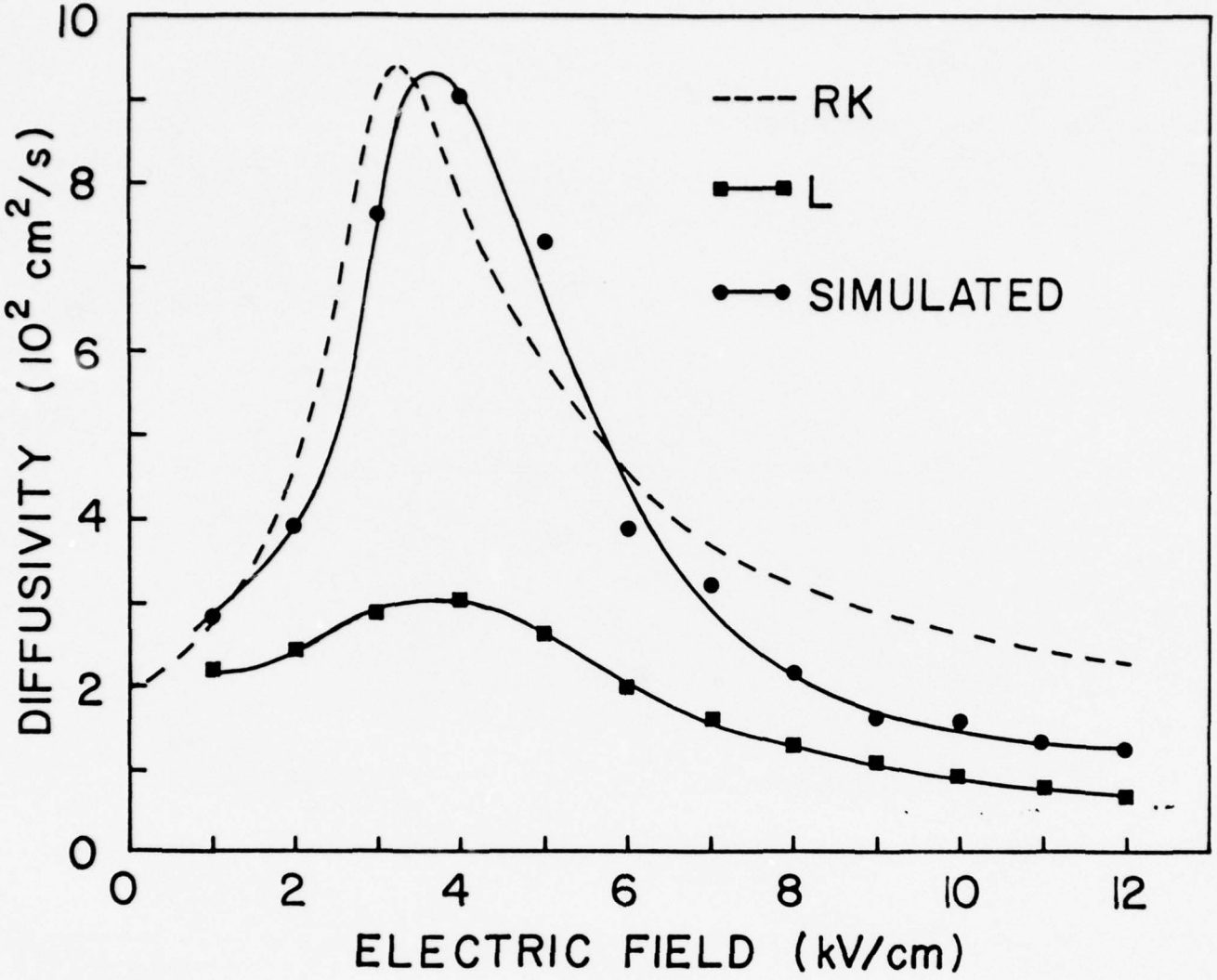
DIFFUSIVITY (10^2 cm^2/s)
ELECTRIC FIELD (kV/cm)
RK
L
SIMULATED
0
2
4
6
8
10
12

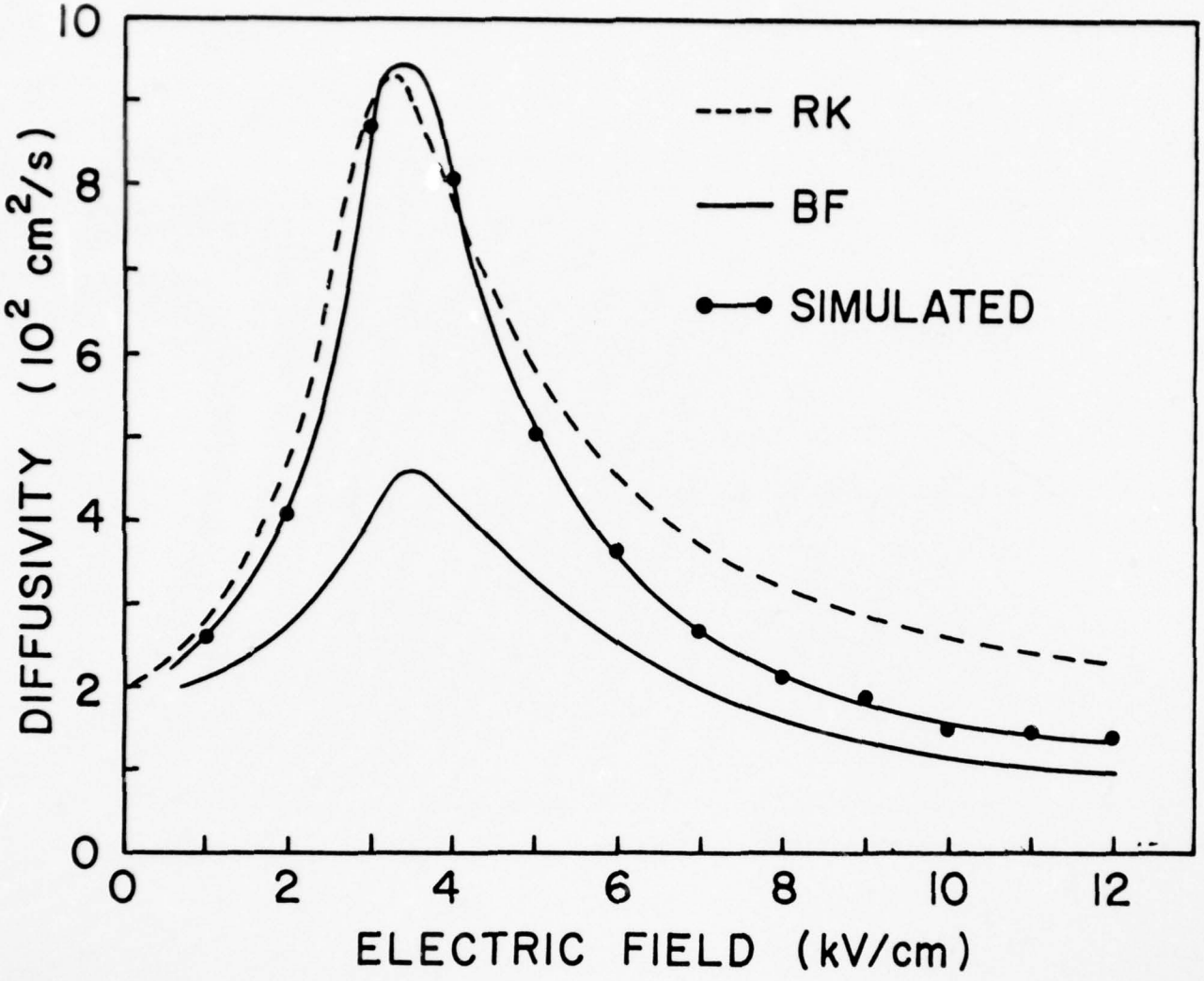
10
8
6
4
2
0
DIFFUSIVITY (10^2 cm^2/s)
RK
BF
SIMULATED
0
2
4
6
8
10
12
ELECTRIC FIELD (kV/cm)

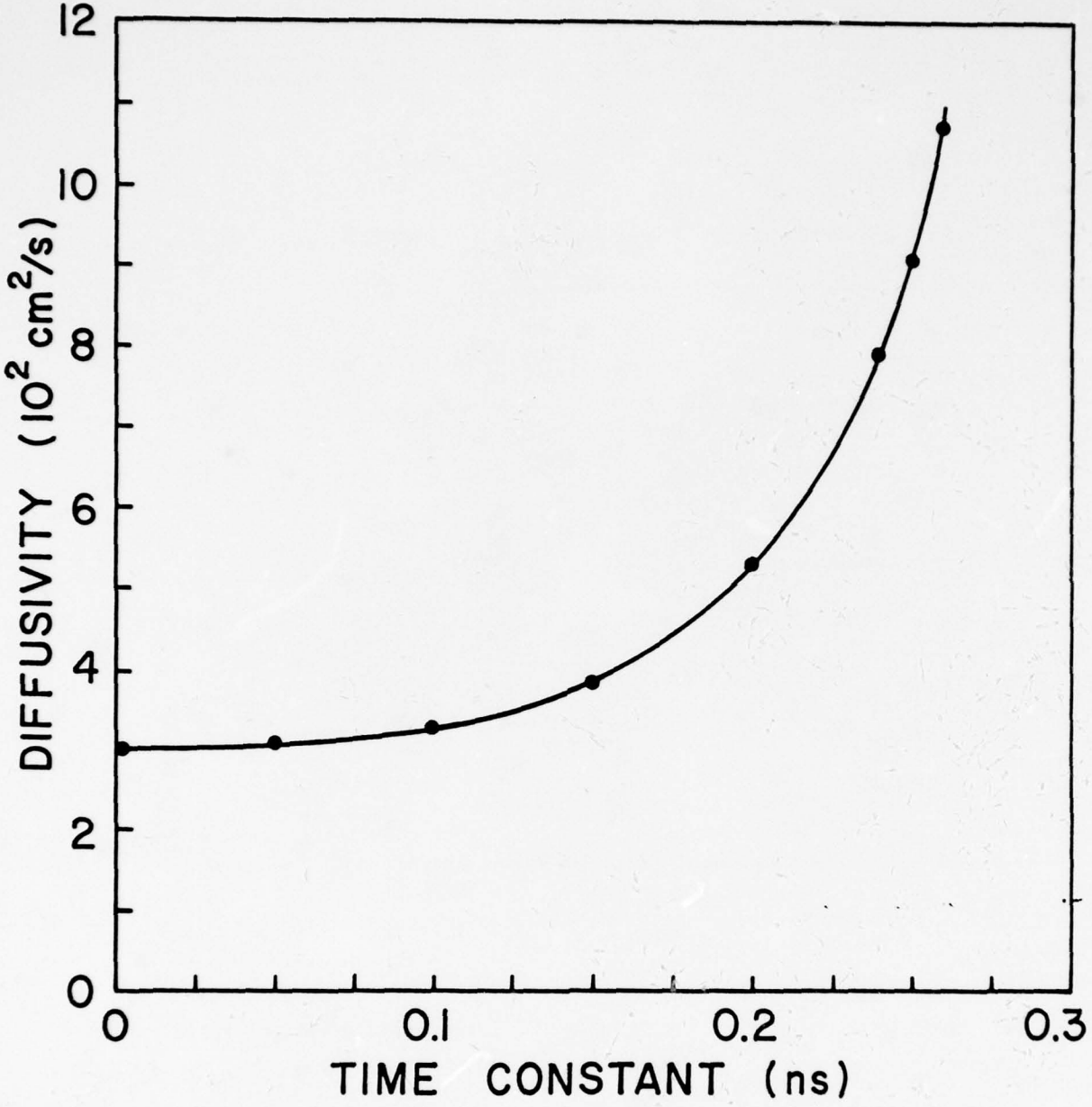
12
10
8
6
4
2
0
DIFFUSIVITY (10^2 cm^2/s)
0
0.1
0.2
0.3
TIME CONSTANT (ns)

Inst. Phys. Conf. Ser. No. 45: Chapter 3 239

Carrier compensation and alloy scattering in $Ga_{1-x}In_xP_{1-y}As_y$ grown by liquid-phase epitaxy

M A Littlejohn, R A Sadler, T H Glisson and J R Hauser
Electrical Engineering Department, North Carolina State University, Raleigh, North Carolina, USA

Abstract. Carrier mobilities achieved experimentally in $Ga_{1-x}In_xP_{1-y}As_y$ alloys are considerably less than those predicted by Monte Carlo transport calculations. In this paper, a comparison between the temperature dependence of electron Hall mobility measured experimentally on LPE-grown samples and calculated from a Monte Carlo method is presented. The experimental data is obtained from samples which are n-type and are grown on semi-insulating InP substrates. The theoretical calculations are based on a diffusion coefficient estimator for calculation of Hall mobility. An analysis of the data indicates that both alloy scattering and carrier compensation are necessary to explain the observed temperature dependence of the Hall mobility.

1. Introduction

The III–V quaternary alloy $Ga_{1-x}In_xP_{1-y}As_y$ has received considerable attention recently due to many desirable electronic and material properties, and this compound has been used in a wide variety of device-related studies (Clawson 1978). In spite of the wide variety of developed applications, the desirable transport properties proposed for this material based on calculations using the Monte Carlo method (Littlejohn *et al* 1977a) have not been fully realized (Morkoc *et al* 1978, Houston *et al* 1978). In particular, the reported Hall mobilities have been considerably lower than predicted, and room-temperature electron concentrations below about 1×10^{16} cm^{-3} have been difficult to achieve. Much of the work has been done using liquid-phase epitaxy (LPE). However, the electron concentrations are much larger for the quaternary than those usually achieved for LPE growth of the binary compounds GaAs and InP, even though the starting constituent source materials used to grow the quaternary are of the same purity as those used for growth of the binaries.

In this paper a comparison between experimental Hall mobilities of LPE-grown quaternary layers on InP substrates and those calculated from the Monte Carlo method is presented. Based on this comparison, it is concluded that both carrier compensation as well as alloy scattering are contributing to the low-field Hall mobility and to its temperature dependence.

2. Experimental aspects

The samples studied in this paper were grown by liquid-phase epitaxy at 660 °C in a standard horizontal slider system (Phatak and Harrison 1978 private com-

0305-2346/79/0045-0239$02.00

munication). The as-grown layers were undoped, and the substrate material was semi-insulating Fe-doped InP in a (111)B orientation. Typical layer thicknesses were around 10 μm. The Hall measurements were made in a variable-temperature cryostat between 77 and 300 K. A standard Van der Pauw sample geometry was used, and contacts to the samples were made with an In–Sn alloy (Houston *et al* 1978).

3. Monte Carlo calculations

The calculations presented in this paper were obtained by the Monte Carlo method, using a programme described previously (Littlejohn *et al* 1977a). Of particular importance is the method used to obtain the quaternary material parameters for $Ga_{1-x}In_xP_{1-y}As_y$. This is done by an interpolation procedure which is based on an assumed knowledge of the constituent binary material parameters of, in this case, GaAs, InAs, InP and GaP. While much needs to be done to validate further this interpolation procedure, it has proved useful in calculating energy band gap and lattice constant (Glisson *et al* 1978, Moon *et al* 1974) as well as electron effective mass (Restorff *et al* 1978). In these cases it has led to good agreement with experimental data. Figure 1 shows the results of a calculation for the Γ valley electron

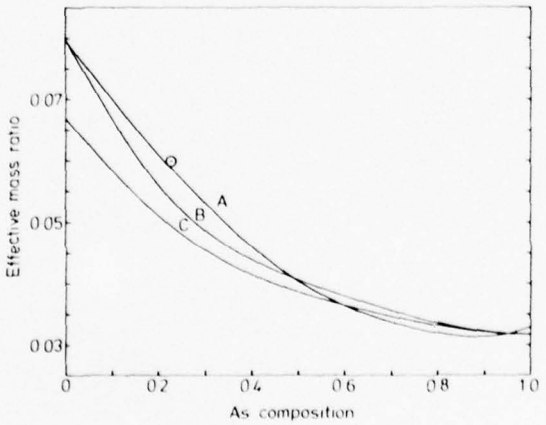

Figure 1. Effective mass ratio as a function of As composition in $Ga_{1-x}In_xP_{1-y}As_y$ lattice-matched to InP. Curve A uses binary effective masses from Restorff *et al* (1978). Curves B and C use values from Littlejohn *et al* (1977a), with two different reported values for InP. ⊙ Restorff *et al* (1978).

effective mass in $Ga_{1-x}In_xP_{1-y}As_y$ as a function of As composition for layers lattice-matched to InP. The three different curves represent calculations based on different values of binary material parameters. However, for $y \geq 0{\cdot}5$ the effective mass does not strongly depend on the uncertainty in the InP effective mass ($y = 0$) (Maloney and Frey 1977). While the more accepted value of effective mass for InP is $0{\cdot}08\ m_0$, another value of $0{\cdot}067\ m_0$ has been used in previous transport calculations (Rode 1970) and is shown in figure 1 for completeness. Also, a very recent measurement of effective mass in $Ga_{0{\cdot}47}In_{0{\cdot}53}As$ has been reported as $0{\cdot}041\ m_0$, and the interpolation procedure illustrated in figure 1 has been questioned (Pearsall *et al* 1979). This measurement was made at near-helium temperatures from Shubnikov–

de Haas oscillation amplitudes, in the same manner as the measurements of Restorff *et al* (1978). At such low temperatures the conduction band density of states is well below 10^{16} cm^{-3}, and one would expect degenerate statistics to be prevalent under the measurement conditions. Thus, this measured effective mass could be larger than the band-edge effective mass shown in figure 1 due to non-parabolic band effects. In fact, on another more heavily doped $Ga_{0.47}In_{0.53}As$ specimen, an effective mass of 0·074 m_0 was measured. This increase was attributed to non-parabolic band effects (Pearsall *et al* 1979). In addition, one would expect a decrease in effective mass with increasing temperature, which would tend to reduce the helium temperature value of 0·041 m_0 to a value possibly more consistent with the value of 0·033 m_0 shown in figure 1 for $Ga_{0.47}In_{0.53}As$. The experimental effective mass data and the calculated values shown in figure 1 appear to be consistent at this point in time.

In general, the Monte Carlo method is difficult to apply with good statistical accuracy at low fields and low temperatures. However, this problem can be overcome to a large extent by using statistical estimators for the diffusion coefficient (Canali *et al* 1975). In addition, the present programme has been further modified to include the effects of heavy doping as well as to use crossed electric and magnetic fields for the computation of Hall mobility, since it is Hall mobility and not drift mobility that is usually measured. The programme details will be presented elsewhere. Heavy doping effects can be important in $Ga_{1-x}In_xP_{1-y}As_y$ alloys having small effective masses such as shown in figure 1. For GaAs, with $m^* = 0{\cdot}067\ m_0$, the conduction band effective density of states is about 4×10^{17} cm^{-3} at 300 K. From the values in figure 1, a number of $1{\cdot}65 \times 10^{17}$ cm^{-3} for the density of states of a quaternary with $y = 0{\cdot}7$ is calculated. As the temperature is decreased to 77 K, the conduction band effective density of states is reduced to 5×10^{16} cm^{-3} for GaAs and to $2{\cdot}1 \times 10^{16}$ cm^{-3} for the quaternary. Thus one could expect degenerate statistics to be important in determining the quaternary transport properties for presently achievable doping levels.

The Monte Carlo method has the additional feature that very detailed transport and scattering factors can be included in the calculations. These factors include such band structure effects as p-state mixing and band non-parabolicity (Fawcett *et al* 1970). Also, the Monte Carlo method takes into account thermal stimulation at temperatures above 300 K of carriers into higher-lying conduction band minima (Rode 1975). If care is taken in assuring statistically accurate estimates in the Monte Carlo method, then the technique should be accurate and very complete, and as convenient as techniques based on classical transport analysis and the use of other numerical methods (Rode 1975).

4. Discussion

The use of the Monte Carlo method for calculating Hall mobility was first examined by considering data for GaAs, since it was felt that values for all important transport coefficients and material parameters were reasonably well known (Rode 1975, Littlejohn *et al* 1977b, Kratzer and Frey 1978). Figure 2 shows Hall mobility as a function of free-electron concentration for GaAs at 300 K for a compensation ratio of 1 (that is, $(N^+ + N^-)/n = 1$, where N^+ is the ionized donor density, N^- is the

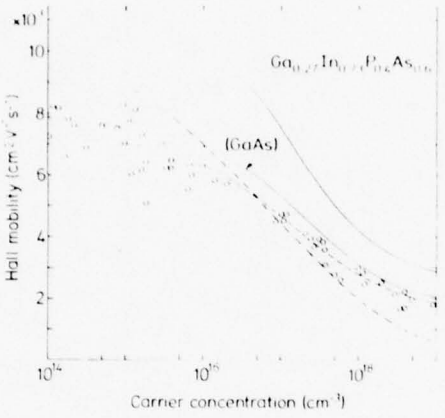

Figure 2. Hall mobility against free-carrier concentration for a compensation ratio of 1. ——— Monte Carlo calculations; – · – · – iterative integral calculations (Rode 1975), – – – – – – data from Sze (1969), ⊙ other experimental data.

ionized acceptor density and n is the free-electron density). Shown for comparison in this figure is a range of experimental data, taken for convenience from the last two proceedings of this conference and the standard data from Sze (1969). Care was taken to record only data reported as Hall mobility data. Also shown are the results of a calculation for Hall mobility based on an iterative integral method (Rode 1975). There are some discrepancies between these two approaches, as can be seen in this figure. For low carrier concentrations the discrepancies (about 13%) can be attributed to slightly different values of bulk material parameters used in the two calculation methods. The material parameters used here in the Monte Carlo calculation have been chosen based on both low-field mobility values and on high-field transport properties (Littlejohn *et al* 1977b, Kratzer and Frey 1978). However, the Monte Carlo method will yield Hall mobilities at low carrier concentrations ($< 10^{14}\,cm^{-3}$) well above $9000\,cm^2\,V^{-1}\,s^{-1}$ if slight adjustments in bulk parameters are made, and certainly the sensitivity of the Hall mobility in pure GaAs to slight variations in material parameters is well recognized (Rode 1975). At high carrier concentrations ($> 10^{16}\,cm^{-3}$) the deviations between these two computational methods are much more subtle. They are due to the way in which the ionized impurity scattering rate is corrected for degeneracy in the Monte Carlo method, and this will be a subject for a future paper. However, in spite of the differences, the authors believe that the Monte Carlo method is an accurate technique for calculating Hall mobility which gives agreement with experimental data over a wide range of carrier concentrations.

Figure 3 shows experimental Hall mobility data against temperature for pure GaAs, along with the calculated temperature dependence of mobility based on both the iterative integral and the Monte Carlo method. Here the Monte Carlo method gives an excellent fit over the temperature range 150–600 K, while Rode (1975) has pointed out that the iterative integral lies about 10% above the experimental data in this range. While we have not done so in this study, it should be pointed out that the Monte Carlo method can be extended to temperatures below 10 K (Canali *et al* 1975). Also, other GaAs material grown in our laboratories has been successfully

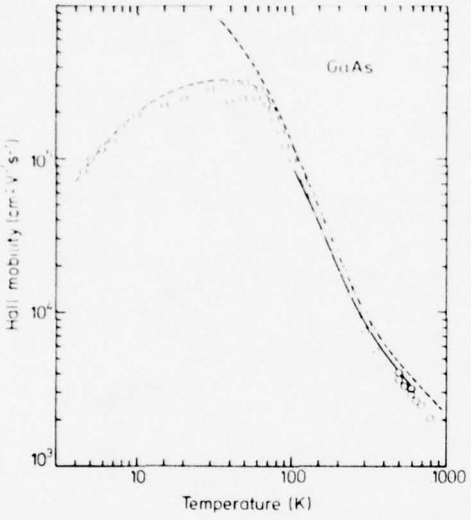

Figure 3. Hall mobility against temperature. ——— Monte Carlo calculations, - - - - and ⊙, iterative integral calculations and experimental data from Rode (1975).

studied by the Monte Carlo method, and the general use of the method appears to be well justified.

Shown in Figure 2 is a calculation of the Hall mobility against electron concentration at 300 K for $Ga_{0.27}In_{0.73}P_{0.4}As_{0.6}$ based on the Monte Carlo method and the material parameter interpolation procedure described previously (Littlejohn *et al* 1977a). At the present time, to the authors' knowledge, the largest value of room-temperature Hall mobility for any quaternary is about 6000 $cm^2 V^{-1} s^{-1}$ with an electron concentration of about 7×10^{15} cm^{-3} (Houston *et al* 1978). Figure 4 shows a summary of typical Hall mobility against temperature for the quaternary (and the InP lattice-matched ternary $Ga_{0.47}In_{0.53}As$) taken in our laboratory and reported in the literature (Houston *et al* 1975, Takeda *et al* 1976). In general, the room-temperature Hall mobilities seem to lie in the range 3000–4000 $cm^2 V^{-1} s^{-1}$,

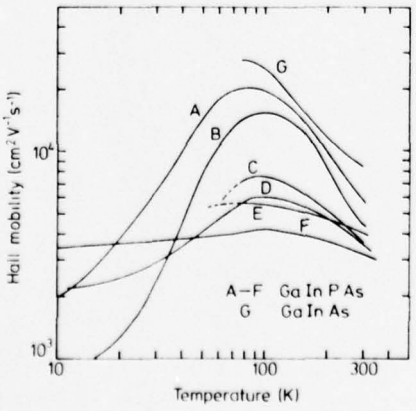

Figure 4. Typical Hall mobility data against temperature for $Ga_{1-x}In_xP_{1-y}As_y$. The curves show data from Houston *et al* (1978), Takeda *et al* (1976), and from this study.

with electron concentrations of $(2-4)\times 10^{16}$ cm^{-3}. Interestingly enough, the highest mobilities and lowest electron concentrations consistently seem to occur near the ternary boundaries for the quaternary, that is, for either relatively low As or P compositions. This is suggestive of the influence of alloy scattering (Littlejohn *et al* 1978).

To investigate the general problem of carrier compensation and alloy scattering in the quaternary $Ga_{1-x}In_xP_{1-y}As_y$, the Monte Carlo method was used to study several typical samples. Figure 5 illustrates the situation when an attempt was made to fit the

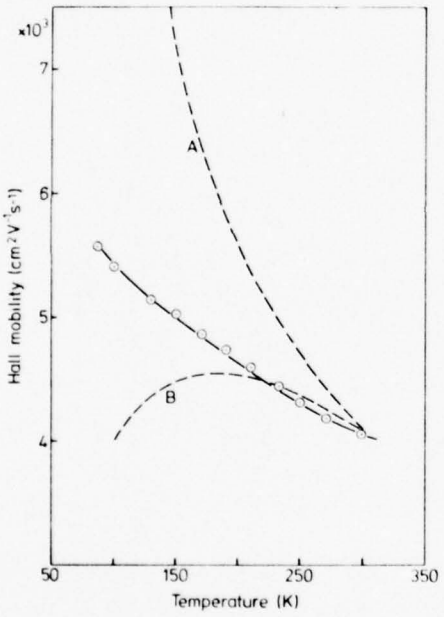

Figure 5. Hall mobility against temperature for $Ga_{0.3}In_{0.7}P_{0.46}As_{0.54}$. The dotted points are experimental data while curves A and B represent Monte Carlo calculations with no carrier compensation and no alloy scattering, respectively.

data using either carrier compensation with no alloy scattering, or alloy scattering with no carrier compensation. First, the alloy scattering potential (Littlejohn *et al* 1978) was varied while keeping the compensation ratio equal to 1(i.e. $N^+ + N^- = n$) until agreement was obtained between the measured and calculated Hall mobility at room temperature. Then the temperature dependence of Hall mobility was calculated, resulting in curve A of figure 5 which is in very poor agreement with the data. Curve B results by removing alloy scattering from the calculation. First, the ionized impurity density was varied until agreement was achieved with the measured Hall mobility at room temperature, while keeping the free-carrier density equal to its measured room-temperature value. Curve B is the resulting temperature variation of Hall mobility with only carrier compensation present. Again the agreement with experimental values at other temperatures is very poor, and it was concluded that neither alloy scattering nor carrier compensation could account for the measured temperature dependence of Hall mobility.

Next, an attempt was made to find a consistent set of values for both the alloy scattering potential and the ionized impurity density which would together give a good fit to the temperature dependence of Hall mobility. To do this two experimental points were chosen, one at 300 K, and one at about 150 K. A detailed parameter study was made by varying the alloy scattering potential and ionized impurity density until a set of values for these two parameters which agreed with the measured values of both Hall mobility and electron concentration at the two temperature extremes. Then the complete Hall mobility against temperature curve was calculated using these values. The results are shown in figure 6. The Monte Carlo estimates lie within

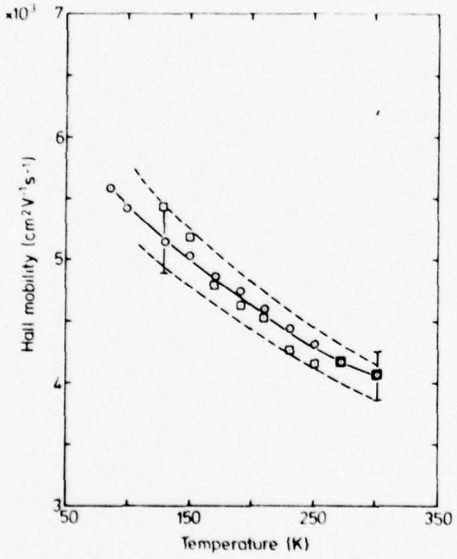

Figure 6. Experimental data and Monte Carlo calculations of Hall mobility against temperature for $Ga_{0.3}In_{0.7}P_{0.46}As_{0.54}$ showing fitted material parameters. $N_D = 7{\cdot}7 \times 10^{16}$ cm^{-3}; $N_A = 5{\cdot}5 \times 10^{16}$ cm^{-3}; $E_A = 0{\cdot}76$ eV; compensation ratio = 3·9.

the broken curves (several estimates were made at each temperature) while the bars indicate a 5% variation in the experimental data at the two temperature extremes. It should be pointed out that the fits are facilitated by the fact that the electron concentration does not vary significantly for these quaternary samples between 100–300 K. The compensation ratio of 3·9 is very close to a sample with a very similar temperature dependence of mobility studied by Houston *et al* (1978).

The calculations are more sensitive to the ionized impurity density than they are to the alloy scattering potential. Thus, it is not feasible to draw many conclusions from the actual value of the alloy scattering parameter shown in figure 6. The value is larger than the proposed theoretical values for three different models (Littlejohn *et al* 1978) by as much as 20 to 100%. There is another scattering mechanism which has the same temperature dependence on mobility as alloy scattering, which is often called space-charge scattering (Weisberg 1962). If this mechanism were also present in these samples it would be difficult to detect from Hall measurements alone, but could effect the determination of the alloy scattering potential by the technique used

here. This added effect could be the result of precipitates, clustering, or other types of second-phase defects.

Other samples with similar Hall mobility temperature dependences have been studied with very similar results as given in figure 6. In all cases, the alloy scattering potential required to fit the data was larger than the theoretical value. Also, for a given compensation ratio, a weaker temperature dependence of mobility is indicative of a larger effect due to alloy scattering. This is not inconsistent with figure 5, since there the room-temperature mobility was used as the target value to be fitted by varying only a single parameter; either the compensation ratio or the alloy scattering potential.

It is interesting to consider those samples with a stronger temperature dependence in this temperature range. Figure 7 shows the results for a $Ga_{0.47}In_{0.53}As$ sample,

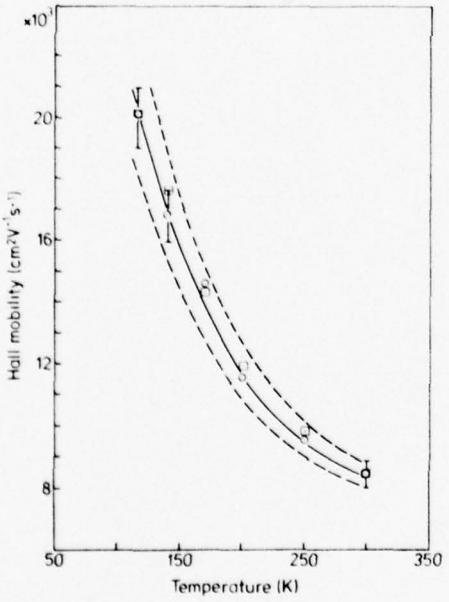

Figure 7. Experimental data and Monte Carlo calculations of Hall mobility against temperature for $Ga_{0.47}In_{0.53}As$ showing fitted material parameters. $N_D = 1{\cdot}5 \times 10^{16}\,cm^{-3}$; $N_A = 1{\cdot}0 \times 10^{16}\,cm^{-3}$; $E_A = 0{\cdot}4$ eV; compensation ratio = 4·8.

which is a ternary in this quaternary system having a Hall mobility at room temperature larger than $8000\,cm^2\,V^{-1}\,s^{-1}$ (Morkoc 1978, Takeda 1978). For this case, the temperature dependence of Hall mobility could be fit by the Monte Carlo method, but with an alloy scattering potential essentially the same as that predicted by the theoretical model. The influence of alloy scattering in this ternary is less important in determining the Hall mobility than it is in the quaternary. This fact is somewhat surprising based on previous results for the scattering potentials in both ternary and quaternary alloys (Littlejohn *et al* 1978).

5. Conclusions

Alloy scattering appears to play an important role in the low-field transport properties of $Ga_{1-x}In_xP_{1-y}As_y$. This conclusion is based on the data and calculations presented in this paper, as well as on other published Hall-effect data. However, the accuracy of the calculations is predicated on the material parameter interpolation procedure, which is presently required for any transport calculations in this quaternary. Historically, the Monte Carlo method has become more useful in studying transport properties in compound semiconductors as accurate material parameters become available. The determination of the basic material parameters should be an important part of programmes which attempt to obtain high-purity $Ga_{1-x}In_xP_{1-y}As_y$ quaternary alloys.

6. Acknowledgments

The authors gratefully acknowledge the financial support of this work by the Office of Naval Research, Arlington, VA, and the Air Force Office of Scientific Research, Washington, DC.

References

Canali C, Jacoboni C, Nava F, Ottoviani G and Alberigi-Quaranta A 1975 *Phys. Rev.* **B12** 2265–84

Clawson A R 1978 *III–V Semiconductor Quaternary Alloy InGaAsP—A Bibliography* (*Tech. Not.* 373, Naval Ocean Systems Center, San Diego)

Fawcett W, Boardman A D and Swain S 1970 *J. Phys. Chem. Solids* **31** 1963–90

Glisson T H, Hauser J R, Littlejohn M A and Williams C K 1978 *J. Electron. Mater.* **7** 1–16

Houston B, Restorff J B, Allgaier R S, Burke J R, Ferry D K and Antypas G A 1978 *Solid St. Electron.* **21** 91–4

Kratzer S and Frey J 1978 *J. Appl. Phys.* **7** 4064–70

Littlejohn M A, Hauser J R and Glisson T H 1977a *Appl. Phys. Lett.* **30** 242–4

—— 1977b *J. Appl. Phys.* **48** 4587–90

Littlejohn M A, Hauser J R, Glisson T H, Ferry D K and Harrison J W 1978 *Solid St. Electron.* **21** 107–14

Maloney T J and Frey J 1977 *J. Appl. Phys.* **48** 781–7

Moon R L, Antypas G A and James L W 1974 *J. Electron. Mater.* **3** 635–43

Morkoc H, Andrews J T, Houng Y M, Sankaran R, Bandy S G and Antypas G A 1978 *Electron. Lett.* **14** 448–9

Pearsall T P, Bisaro R, Merenda P, Laurencin G, Ansel R and Portal J C 1979 this volume

Restorff J B, Houston B, Burke J R and Hayes R E 1978 *Appl. Phys. Lett.* **32** 189–90

Rode D L 1970 *Phys. Rev.* **B2** 1012–24

—— 1975 *Semiconductors and Semimetals* Vol. 10 (New York: Academic Press) p 1

Sze S M 1969 *Physics of Semiconductor Devices* (New York: Wiley) p 40

Takeda Y, Sasaki S, Imamura Y and Takagi T 1976 *J. Appl. Phys.* **47** 5405–8

Weisberg L R 1962 *J. Appl. Phys.* **33** 1817–28

MONTE CARLO CALCULATION OF HALL MOBILITY AND VELOCITY-FIELD CHARACTERISTICS FOR HEAVILY-DOPED GAAS

C.K. Williams, T.H. Glisson, J.R. Hauser, M.A. Littlejohn

North Carolina State University
Electrical Engineering Department
Raleigh, North Carolina 27650

October 4, 1979

A method of including the Pauli Exclusion Principle in the Monte Carlo procedure is presented. The procedure is then used to calculate the Hall mobility and velocity-field characteristics for GaAs with impurity concentrations up to 10^{19} cm^{-3}.

Introduction

The Monte Carlo technique, first described by Kurosawa[1] and then generalized by Fawcett et al[2], has become a very important tool in predicting semiconductor material characteristics. While it has been used to analyze many different materials, it is usually restricted to nondegenerate cases. To remove this restriction from the usual Monte Carlo procedure electron-electron scattering and the Pauli Exclusion Principle must be included. Some attempts to include the former have been reported [3-6] and one to include the latter has been reported[7].

In this paper, one method of incorporating the Pauli Exclusion Principle in the Monte Carlo procedure is presented which is valid at low fields. The method presented here differs from that described by S. Bosi and C. Jacoboni[7] in that (1) an estimate of the probability of occupancy is used instead of accumulating this information via a k-space mesh during the simulation and (2) ionized impurity interaction is treated as a special case. This method is used to calculate the low field Hall mobility of GaAs. An extension of this method is then used to determine the velocity-field characteristics of GaAs. Both calculations are done for both nondegenerate and degenerate cases.

The Monte Carlo model used in this work is the same as that described elsewhere [8,9] except the present model includes p-state mixing. Briefly, it incoporates a three valley model with nonparabolicity, and acoustic phonon, optical phonon, ionized

impurity, polar optical, piezoelectric, and intervalley scattering processes. The material parameters used for GaAs are the same as those presented in [10] and are repeated in Table 1 for completeness.

Corrections to Scattering Rates

The Pauli Exclusion Principle must be considered in modelling degenerate semiconductors. To include the Pauli Exclusion Principle in the Monte Carlo procedure described in the previous section, we multiply the scattering rate $S_n(\mathbf{k},\mathbf{k}')$ between two wave-vector states $\mathbf{k}$ and $\mathbf{k}'$ by the factor $(1-f(\mathbf{k}'))$. Here $f(\mathbf{k}')$ is the probability the final state $\mathbf{k}'$ is occupied so that $(1-f(\mathbf{k}'))$ is the probability the state is unoccupied. Thus, the total scattering rate from the state $\mathbf{k}$ due to the n'th process is

$$\lambda_n(\vec{k}) = \int d\vec{k}' \; S_n(\vec{k},\vec{k}')(1-f(\vec{k}')). \tag{1}$$

For low fields, the occupation probability distrubition $f(\mathbf{k})$ is near equilibrium, so that

$$f(\vec{k}) \simeq f_o(\vec{k}) \tag{2}$$

where $f_o(\mathbf{k})$ is the equilibrium occupation probability distribution which is the Fermi-Dirac distribution

$$f_o(\vec{k}) = \frac{1}{1+e^{(E(\vec{k})-E_F)/kT}}. \tag{3}$$

In the work reported here, the relationship between the energy E and wave-vector $\mathbf{k}$ in the i'th valley (i=1,2,3) is taken to be [2]

$$\frac{\hbar^2 k^2}{2m_i^*} = E(1+\alpha_i E) = \gamma_i(E) \tag{4}$$

where α is the nonparabolicity and m^* is the effective mass.

To correct the scattering rates as in Eq. (1), only the Fermi energy need be calculated. This is done by solving (numerically) the equation [11]

$$n = \frac{\sqrt{2}}{\pi^2 \hbar^3} \sum_{i=1}^{3} M_{ci} \, m_i^{*3/2} \int_{E_{ci}}^{E_{TOPi}} \sqrt{\gamma_i(E)} \; \frac{d\gamma_i(E)}{dE} \, f_o(E) dE \tag{5}$$

where M_{ci} is the number of equivalent minima in the i'th valley and n is the density of conduction band electrons.

Figure 1 shows the scattering rate for polar optical emission with and without the correction factor in the valley for an impurity concentration of 10^{19} cm^{-3} and a temperature of 300 K. In general, the correction factor effectively prohibits scatterings that would result in a final energy less than the Fermi energy.

The correction factor is included in all scattering rates except ionized impurity. An ionized impurity creates a localized perturbation on the electric field. The wave-vector **k** of an electron influenced by this perturbing field is not changed abruptly to **k'** but is gradually changed over the time the carrier is influenced by the perturbing field. Thus, even though an ionized impurity interaction is treated in the Monte Carlo procedure as an instantaneous scattering from wave-vector **k** to **k'**, the correction factor (1-f(**k'**)) seems inappropriate.

Determination of Low Field Hall Mobility

To calculate the Hall mobility using the Monte Carlo procedure, it is necessary to include a magnetic field. For this case the time derivative of the wave-vector **k** is

$$\frac{\partial \vec{k}}{\partial t} = \frac{\vec{F}}{h} = \frac{q}{h} (\vec{\varepsilon} + \vec{v} \times \vec{B}) \tag{6}$$

where $\vec{\varepsilon}$ is the electric field vector, **B** is the magnetic field vector, and **v** is the carrier velocity.

Here the electric field is taken to be in the $\hat{z}$ direction and the magnetic field in the $\hat{x}$ direction. With this configuration the low field Hall mobility is shown in the appendix to be given by

$$\mu_H = \frac{1}{B} \sqrt{\frac{D_x}{D_y} - 1} = \frac{1}{B} \sqrt{\frac{D_x}{D_z} - 1} \tag{7}$$

where D_x, D_y, and D_z are the diffusion coefficients in the $\hat{x}$, $\hat{y}$, and $\hat{z}$ directions, respectively, and B is the magnitude of the magnetic field. Since D_y and D_z are equivalent for low fields, the estimate of μ_H may be improved by using

$$\mu_H = \frac{1}{B} \sqrt{\frac{D_x}{D_{yz}} - 1} \tag{8}$$

where

$$D_{yz} = \frac{1}{2}(D_y + D_z) \tag{9}$$

Using Eqs. (8) and (9) in the Monte Carlo program with a magnetic field, the Hall mobility versus impurity concentration was calculated for GaAs with corrections to the scattering rates as described earlier (no correction to the rate for ionized impurity scattering). Figure 2 shows a simple flow chart of the program used. The calculation was also carried out for two other cases: (1) no correction to the scattering rates, and (2) correction to all the scattering rates (including ionized impurity). The results are given in Fig. 3. Also shown is the experimental data obtained by Sze[12]. Good agreement with Sze's experimental data is obtained by using the correction to all the scattering rates except ionized impurity, while the other two cases give rather poor agreement, supporting the special treatment of the ionized impurity interaction.

Calculation of Velocity-Field Characteristics

The method used above to account for the Pauli Exclusion Principle in the calculation of low field Hall mobility must be modified for the calculation of velocity-field characteristics for degenerate semiconductors. The method adopted here is to assume the probability of occupancy in the i'th valley (i=1,2,3) is

$$f_i(E) = \frac{1}{1+e^{(E-E_{Fi})/kT_{ei}}} \tag{10}$$

Thus a quasi Fermi level E_{Fi} and quasi electron temperature T_{ei} are associated with the carriers in the i'th valley. The correction to the scattering rates in the i'th valley is then based on the probability of occupancy given in Eq. (10).

Incorporating these new features in the Monte Carlo procedure requires an iterative solution for the carrier temperatures and the Fermi energies. Initial values are determined by assuming that (1) the carrier temperatures are all equal to the lattice temperature and (2) the Fermi energies are all equal. Then, Eq. (5) can be solved for the Fermi energy. Using these initial values, the scattering rates are corrected and the carrier is tracked for some specified number of interactions. The density of carriers n_i and the average energy $\bar{E}_i$ in each valley are then calculated. Then

$$n_i = \frac{\sqrt{2}}{\pi^2 h^3} M_{ci} m_i^{*3/2} \int_{E_{ci}}^{E_{TOPi}} \sqrt{\gamma_i(E)} \frac{d\gamma_i(E)}{dE} f_i(E)dE \tag{11}$$

and

$$\bar{E}_i = \frac{\sqrt{2}}{\pi^2 h^3} \frac{M_{ci}\, m_i^{*3/2}}{n_i} \int_{E_{ci}}^{E_{TOPi}} E\sqrt{\gamma_i(E)}\, \frac{d\gamma_i(E)}{dE}\, f_i(E)\, dE \qquad (12)$$

are used to obtain new estimates of the quasi-electron temperatures and the quasi-Fermi energies. The new carrier temperatures and Fermi energies are then used to obtain new correction factors $(1-f(\vec{k}'))$ and new scattering rates and the process is repeated. This process of correcting scattering rates, tracking the carrier, and calculating new estimates of carrier temperatures and Fermi energies is continued until a self-consistent solution is reached, i.e., until successive iterations give little change in E_{Fi} and T_{ei}. Figure 4. shows a flow chart for the iterative procedure for a single valley.

Using the method outlined above in the Monte Carlo procedure, the velocity-field characteristics of GaAs were calculated for impurity concentrations of 10^{16}, 10^{18}, and 10^{19} cm^{-3}. The results are given in Fig. 5. For comparison the velocity-field characteristics for GaAs calculated from the Monte Carlo procedure without including the Pauli Exclusion Principle are shown. For the nondegenerate case, impurity concentration of 10^{16} cm^{-3}, the two curves are in good agreement, while for the two degenerate cases the difference becomes more pronounced. This result is expected since the Pauli Exclusion Principle is important only for the degenerate cases.

Appendix

An expression for the Hall mobility in terms of the diffusion coefficients can be obtained from the current density equation for low fields

$$\vec{J}_n = q\mu_n\vec{\varepsilon} + qD_n\nabla n + \vec{J}_n x(\mu_H\vec{B}) \tag{A1}$$

Let

$$\vec{B}' = \mu_H\vec{B} \tag{A2}$$

and

$$\vec{\varepsilon}' = \vec{\varepsilon} + \frac{1}{n}\frac{D_n}{\mu_n}\nabla n \tag{A3}$$

in terms of which Eq. (A1) can be written

$$\vec{J}_n = q\mu_n n\vec{\varepsilon}' + \vec{J}_n x\vec{B}' \ . \tag{A4}$$

The solution to Eq. (A4) is of the form

$$\vec{J}_n = C_1\vec{\varepsilon}' + C_2\vec{B}' + C_3\,\vec{\varepsilon}'x\vec{B}' \tag{A5}$$

where C_1, C_2, and C_3 are to be determined. Substitution of Eq. (A5) into the right side of Eq. (A4) yields

$$\vec{J}_n = (q\mu_n n - C_3 B'^2)\vec{\varepsilon}' + C_3(\vec{B}'\cdot\vec{\varepsilon}') + C_1\vec{\varepsilon}'x\vec{B}'. \tag{A6}$$

Equating coefficients between Eqs. (A5) and (A6) gives

$$C_1 = \frac{q\mu_n n}{1+B'^2} = C_3 \tag{A7}$$

$$C_2 = \frac{q\mu_n n}{1+B'^2}\,(\vec{B}'\cdot\vec{\varepsilon}') \ . \tag{A8}$$

Thus, Eq. (A6) becomes

$$\vec{J}_n = q\mu' n\left\{\vec{\varepsilon} + \frac{1}{n}\frac{D_n}{\mu_n}\nabla n + \mu_H{}^2[B\cdot(\vec{\varepsilon}+\frac{1}{n}\frac{D_n}{\mu_n}\nabla n)]\vec{B} + \mu_H(\vec{\varepsilon}+\frac{1}{n}\frac{D_n}{\mu_n}\nabla n)x\vec{B}\right\} \tag{A7}$$

where

$$\mu' = \frac{\mu_n}{1+(\mu_H B)^2} \tag{A8}$$

For the case where the magnetic field is in the $\hat{x}$ direction and the electric field is in the $\hat{z}$ direction

$$\nabla n \cdot \vec{B} = \frac{\partial n}{\partial x} B, \tag{A9}$$

$$\vec{\varepsilon} \times \vec{B} = - \varepsilon B \hat{y}, \tag{A10}$$

$$\nabla n \times \vec{B} = B \frac{\partial n}{\partial z} \hat{y} - B \frac{\partial n}{\partial y} \hat{z}, \tag{A11}$$

and Eq. (A7) becomes

$$\begin{aligned} \vec{J}_n = {} & qD_n \frac{\partial n}{\partial x} \hat{x} + \frac{qD_n}{1+\mu_H{}^2 B^2} \left(\frac{\partial n}{\partial y} + \mu_H B \frac{\partial n}{\partial z}\right)\hat{y} \\ & - \frac{q\mu_n n(\mu_H B)}{1+\mu_H{}^2 B^2} \varepsilon \hat{y} + \frac{q\mu_n n}{1+\mu_H{}^2 B^2} \varepsilon \hat{z} \\ & + \frac{qD_n}{1+\mu_H{}^2 B^2} \left(\frac{\partial n}{\partial z} - \mu_H B \frac{\partial n}{\partial y}\right) \hat{z} \, . \end{aligned} \tag{A12}$$

Now, assuming the generation and recombination rates are equal, the continuity equation for electrons is

$$\frac{\partial n}{\partial t} = \frac{1}{q} \nabla \cdot \vec{J}_n \tag{A13}$$

Substituting Eq. (A12) into Eq. (A13) yields

$$\frac{\partial n}{\partial t} = v_z \frac{\partial n}{\partial z} + v_y \frac{\partial n}{\partial y} + D_x \frac{\partial^2 n}{\partial x^2} + D_y \frac{\partial^2 n}{\partial y^2} + D_z \frac{\partial^2 n}{\partial x^2} \tag{A14}$$

where

$$v_z = \frac{\mu_n}{1+\mu_H{}^2 B^2} \, , \tag{A15}$$

$$v_y = \frac{-\mu_n \varepsilon (\mu_H B)}{1+\mu_H{}^2 B^2} \tag{A16}$$

$$D_x = D_n \tag{A17}$$

$$D_y = D_z = \frac{D_n}{1+\mu_H{}^2 B^2} \tag{A18}$$

Finally, combining Eqs. (A17) and (A18) yields

$$\mu_H = \frac{1}{B}\sqrt{\frac{D_x}{D_y} - 1} = \frac{1}{B}\sqrt{\frac{D_x}{D_z} - 1} \tag{A19}$$

which is the desired result.

References

1. T. Kurosawa, Proc. Int. Conf. Semicond. Kyoto, J. Phys. Soc. Jpn. Suppl. **21**, 424 (1966).

2. W. Fawcett, A.D. Boardman and S. Swain, J. Phys. Chem. Solids **31**, 1963 (1970).

3. L.B. Montefusco and C. Jacoboni, Solid St. Commun. **10**, 71 (1972).

4. R.C. Curby and D.K. Ferry, Phys. Stat. Sol. (a) **15**, 319 (1973).

5. I. Jager, Phys. Stat. Sol. (b) **61**., 711 (1974).

6. A. Matulionis, J. Pozela and A. Reklaitis, Solid St. Commun. **16**, 1133 (1975).

7. S. Bosi and C. Jacoboni, J. Phys. C **9**, 315 (1976).

8. M.A. Littlejohn, J.R. Hauser, and T.H. Glisson, Appl. Phys. Lett. **26**, 625 (1975).

9. J.P. Hauser, M.A. Littlejohn, and T.H. Glisson, Appl. Phys. Lett. **28**, 458 (1976).

10. M.A. Littlejohn, J.R. Hauser, and T.H. Glisson, J. Appl. Phys. **48**, 4587 (1977).

11. R.H. Bube, Electronic Properties of Crystalline Solids (Academic Press, New York, 1974), pp. 172.

12. S.M. Sze, Physics of Semiconductor Devices (Wiley, New York, 1969), pp. 40.

Table 1. GaAs material parameters used in calculations.

Bulk material parameters

Parameter	Value
Lattice constant	5.642×10^{-8} cm
Density	5.36 g/cm^3
Electron affinity	4.07 eV
Piezoelectric constant	0.16 C/m^2
LO phonon energy	0.03536 eV
Sound velocity	5.24×10^5 cm/sec
Optical dielectric constant	10.92
Static dielectric constant	12.90

Valley-dependent material parameters

	Conduction-band valley		
Parameter	Γ(000)	X(100)	L(111)
Acoustic def. pot. (eV)	7.0	9.27	9.2
Effective mass (m/m)	0.063	0.58	0.222
Nonparabolicity (eV^{-1})	0.610	0.204	0.461
Energy band gap (eV) (relative to valence band)	1.439	1.961	1.769
Optical def. pot. (eV/cm)	0	0	3×10^8
Optical phonon energy (eV)	...	...	0.0343
Intervalley def. pot. (eV/cm)			
from Γ(000)	0	1×10^9	1×10^9
from X(100)	1×10^9	7×10^8	5×10^8
from L(111)	1×10^9	5×10^8	1×10^9
Intervalley phonon energy (eV)			
from Γ(000)	0	0.0299	0.0278
from X(100)	0.0299	0.0299	0.0293
from L(111)	0.0278	0.0293	0.0290
No. equivalent valleys	1	3	4

List of Figures

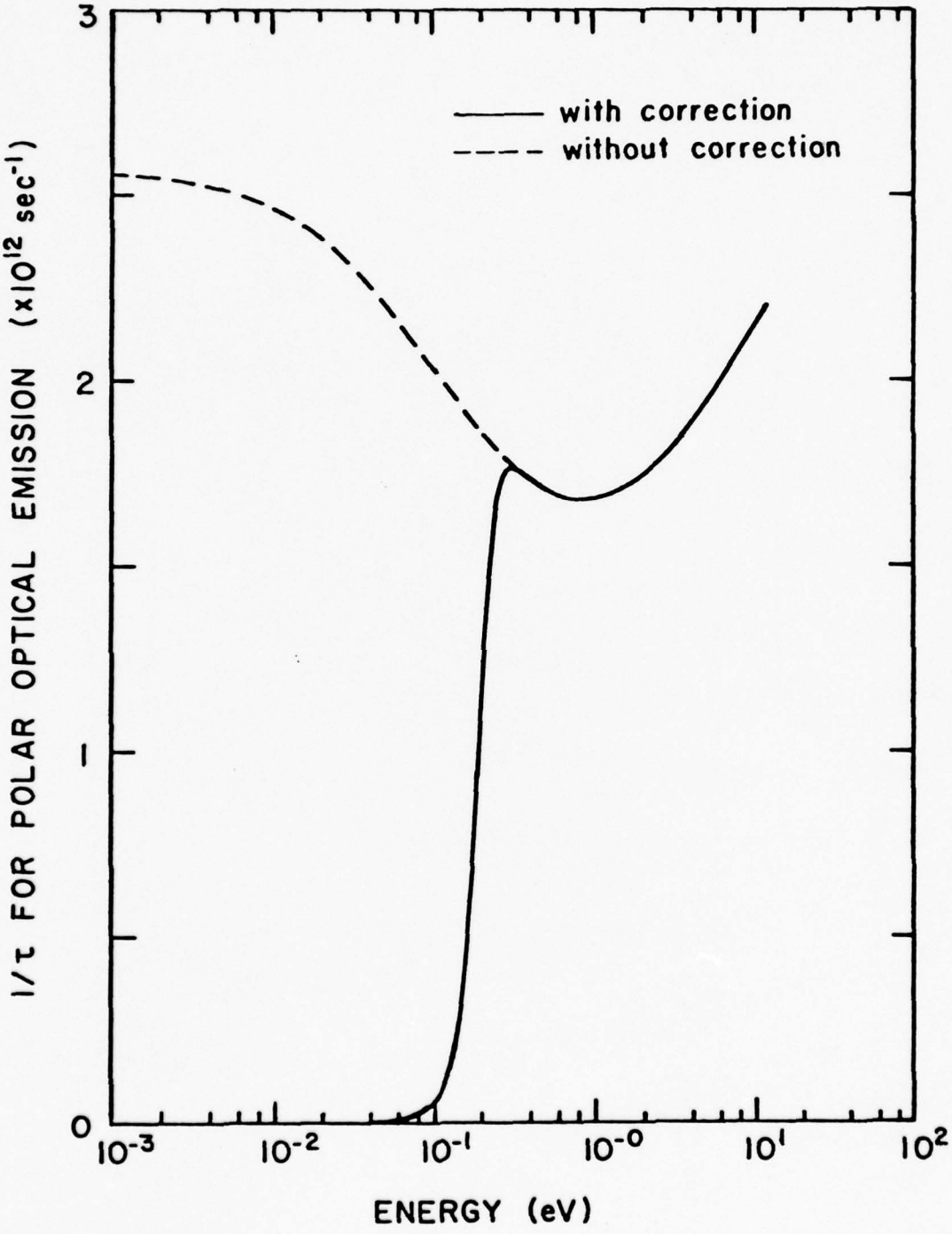
with correction
without correction
1/τ FOR POLAR OPTICAL EMISSION (x10^12 sec^-1)
3
2
1
0
10^-3
10^-2
10^-1
10^-0
10^1
10^2
ENERGY (eV)

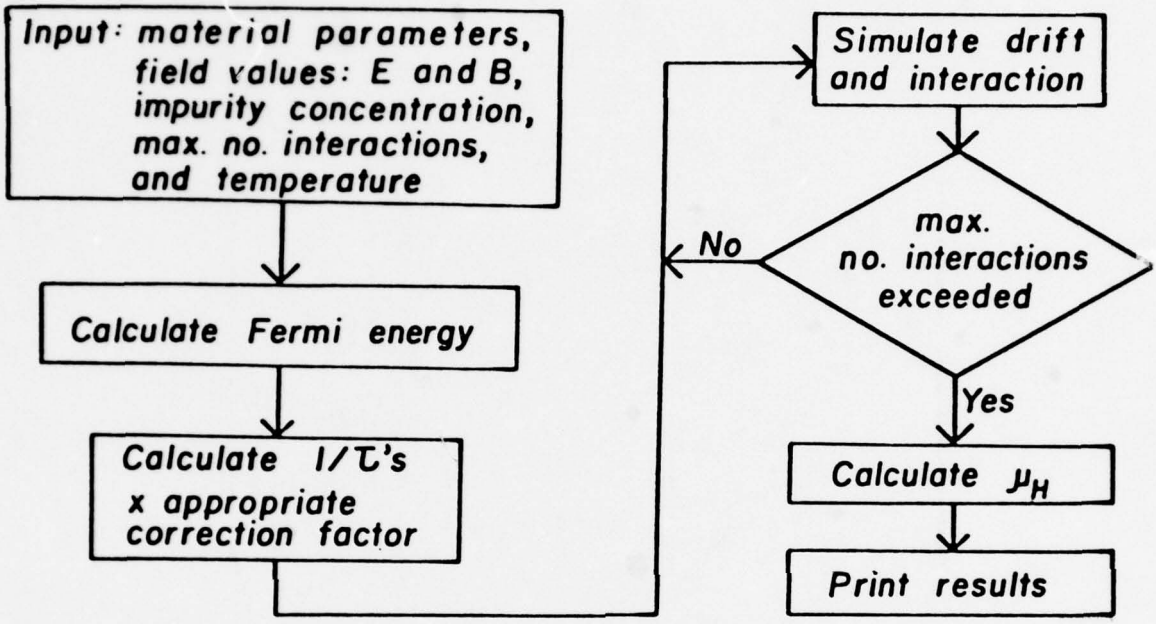
Input: material parameters, field values: E and B, impurity concentration, max. no. interactions, and temperature
Calculate Fermi energy
Calculate 1/τ's x appropriate correction factor
Simulate drift and interaction
max. no. interactions exceeded
No
Yes
Calculate μ_H
Print results

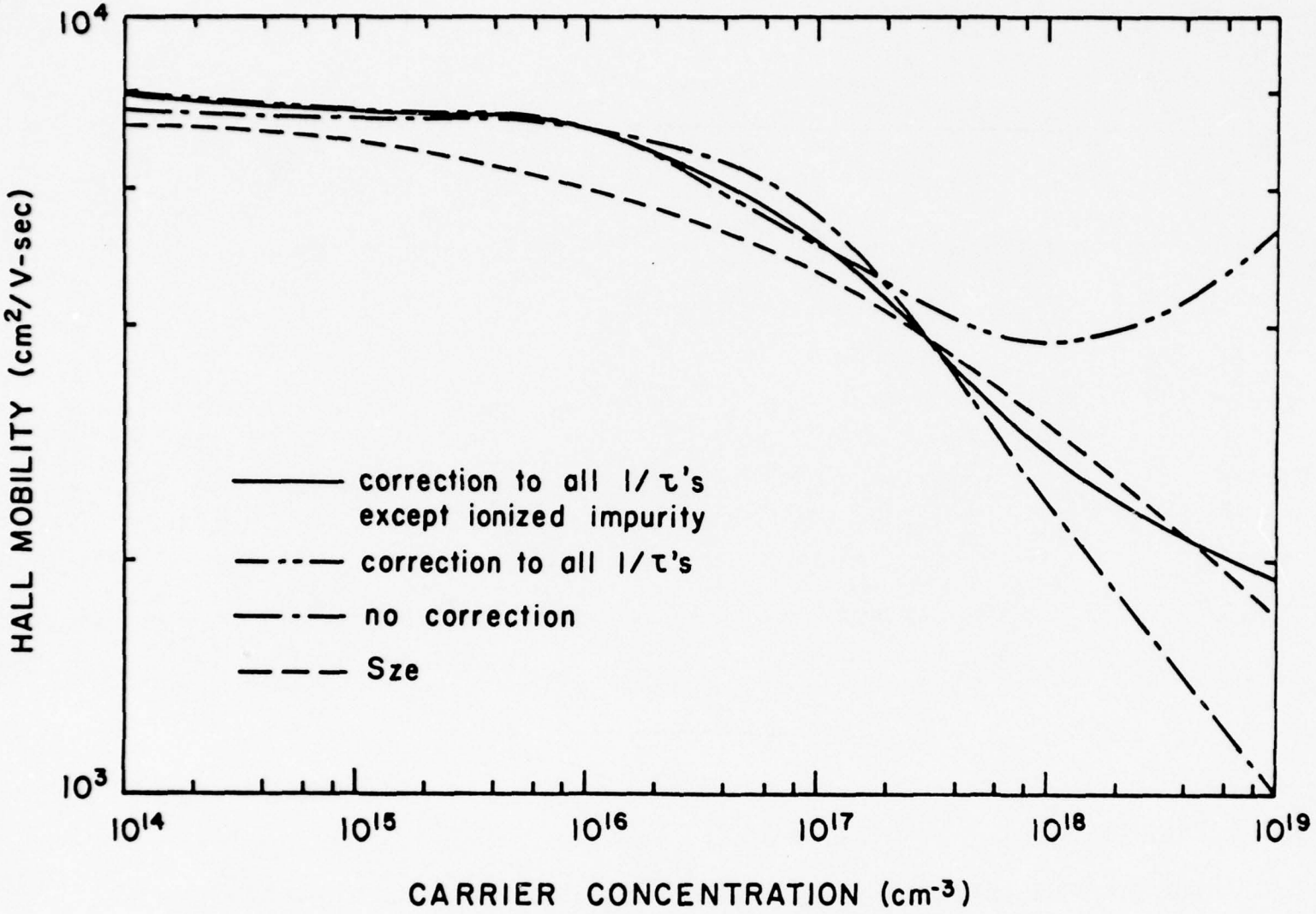
10^4
10^3
HALL MOBILITY (cm^2/V-sec)
correction to all 1/τ's except ionized impurity
correction to all 1/τ's
no correction
Sze
10^{14}
10^{15}
10^{16}
10^{17}
10^{18}
10^{19}
CARRIER CONCENTRATION (cm^{-3})

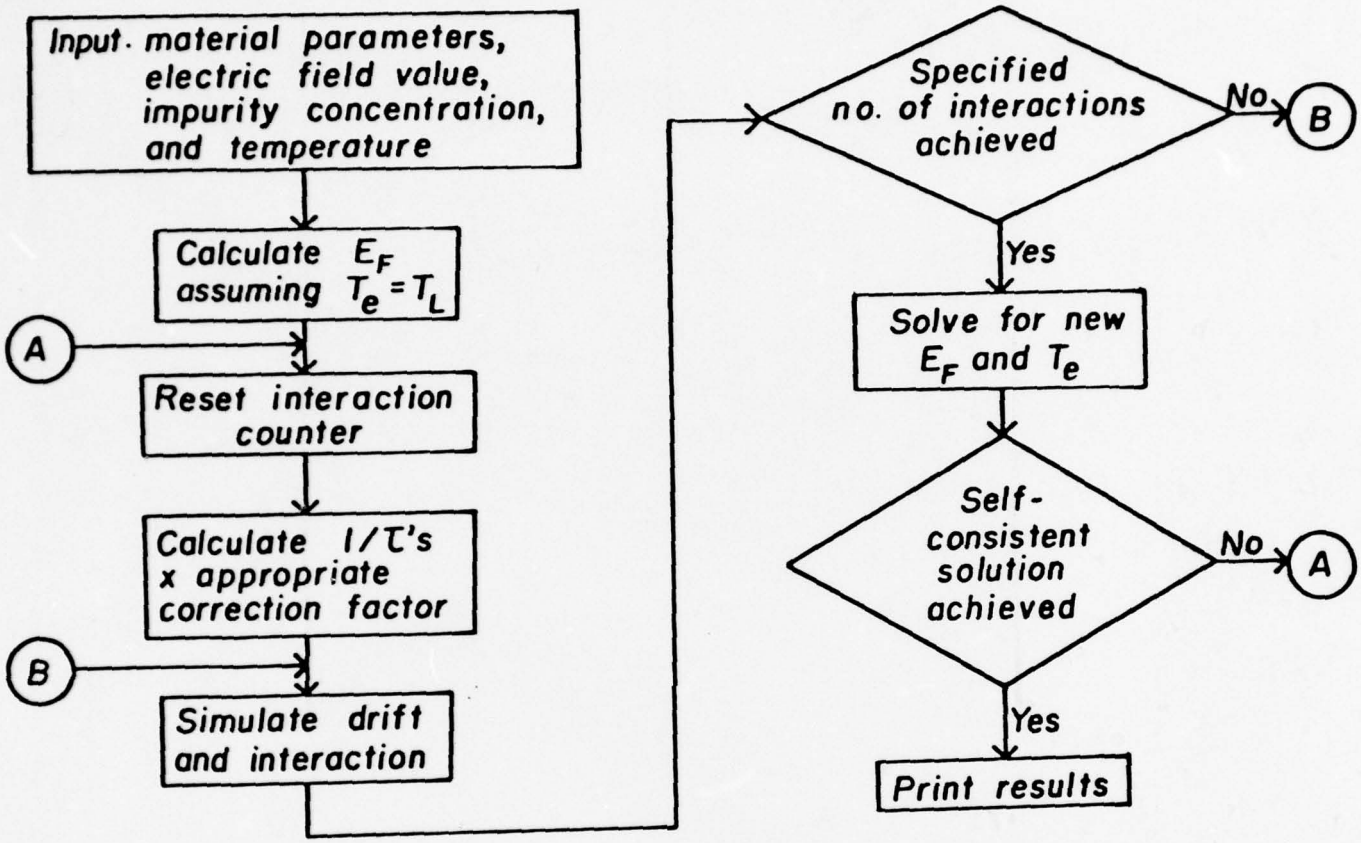
Input material parameters, electric field value, impurity concentration, and temperature
Calculate E_F assuming $T_e = T_L$
A
Reset interaction counter
Calculate $1/\tau$'s x appropriate correction factor
B
Simulate drift and interaction
Specified no. of interactions achieved
No
B
Yes
Solve for new E_F and T_e
Self-consistent solution achieved
No
A
Yes
Print results

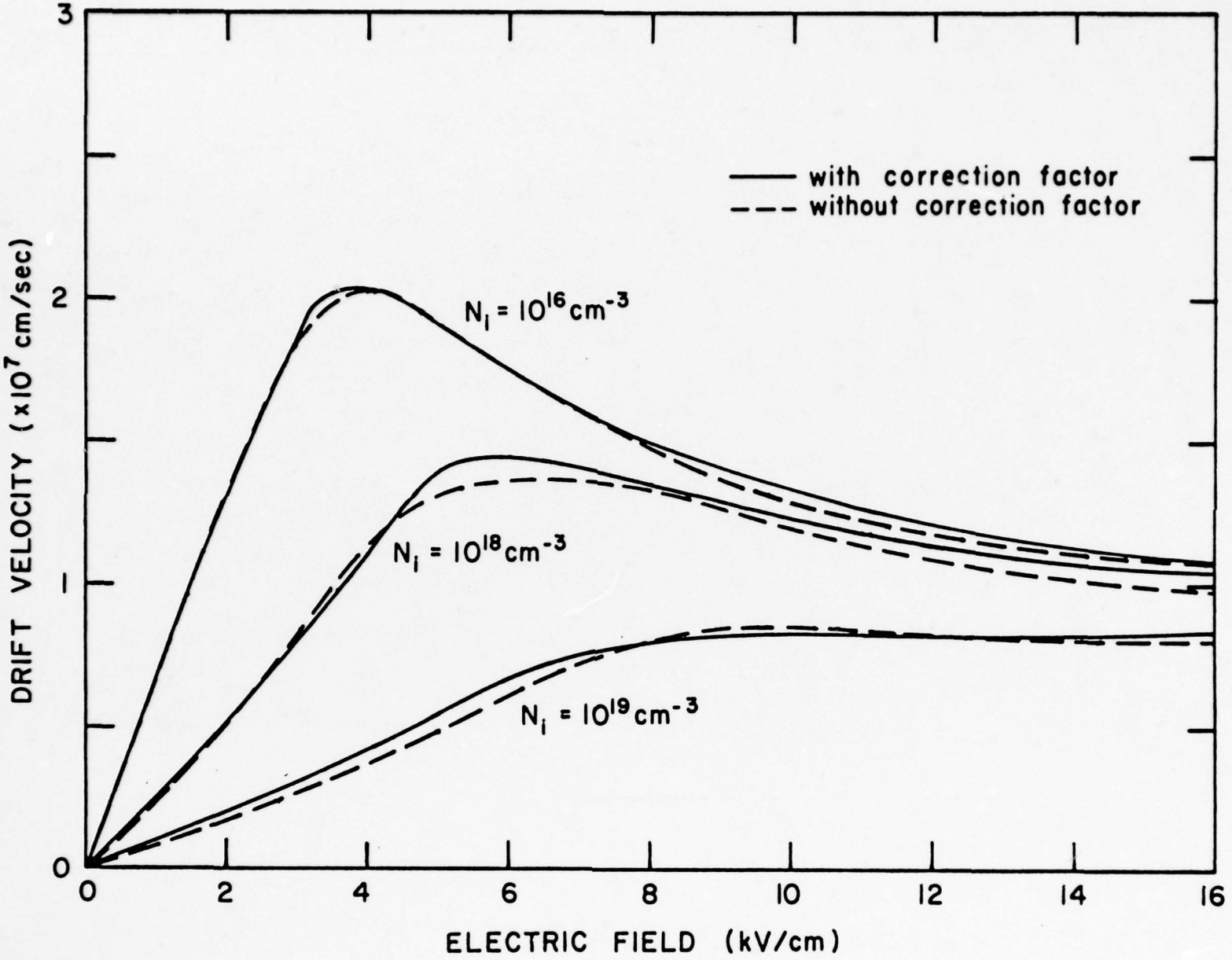
with correction factor
without correction factor
$N_i = 10^{16} cm^{-3}$
$N_i = 10^{18} cm^{-3}$
$N_i = 10^{19} cm^{-3}$
DRIFT VELOCITY ($\times 10^7$ cm/sec)
ELECTRIC FIELD (kV/cm)
0
1
2
3
0
2
4
6
8
10
12
14
16

INFLUENCE OF CENTRAL VALLEY EFFECTIVE MASS AND ALLOY SCATTERING ON TRANSIENT DRIFT VELOCITY IN $Ga_{1-x}In_xP_{1-y}As_y$*

M. A. Littlejohn, L. A. Arledge, T. H. Glisson, and J. R. Hauser
Electrical Engineering Department
North Carolina State University
Raleigh, NC 27650

ABSTRACT

The instantaneous ensemble-averaged and time-averaged velocity of electrons are presented for $Ga_{.27}In_{.73}P_{.4}As_{.6}$, and the results are compared to those for GaAs. The results indicate that both the effective mass in the Γ conduction band and alloy scattering are very critical in determining the transient (or velocity-overshoot) characteristic as well as the static velocity-field characteristic for this quaternary material.

*This work was supported by the Office of Naval Research, Arlington, Virginia, U.S.A.

In a previous publication [1] the static (time-averaged) velocity-field characteristic of the $Ga_{1-x}In_xP_{1-y}As_y$ quaternary alloy was presented. This characteristic was calculated using a monte carlo simulation of the electron transport. The quaternary material properties used in the simulation were obtained by an interpolation procedure based on experimental and theoretical material parameters for the binary constituents of the quaternary. This interpolation procedure for a given material parameter results in a continuous, smoothly-varying function in the (x,y) compositional plane, which reduces to the correct compositional dependence along the ternary boundaries and to the binary values at the corners of the compositional plane.

There have been very few experimental investigations of the basic material properties of $Ga_{1-x}In_xP_{1-y}As_y$, and thus very few means for confirmation of the above-mentioned interpolation procedure. Energy band gap measurements by photoluminescence [2-4] do support the interpolation procedure. However, the drift velocity is affected only very slightly by the value of the band gap. Recently, several techniques have been used to measure the band edge effective mass [5-7], and this parameter fundamentally affects the transport properties of any semiconductor. Some of these measurements do support the interpolation technique [5,6]. However, other experimental data, combined with theoretical calculations, [7] indicate that the effective mass has substantially less "bowing" than is predicted by the interpolation formula [8] for quaternary compositions which are lattice-matched to InP.

Very recently-presented data for both electron mobility [9] and electron effective mass [10] further support this contention.

The purpose of this paper is to examine the influence of central (Γ) valley effective mass on the calculations of both the time-averaged static drift velocity versus electric field intensity, and the ensemble-averaged transient velocity (velocity overshoot) characteristic for $Ga_{1-x}In_xP_{1-y}As_y$. Also, the importance of alloy scattering will be further considered [1]. The calculations are presented for one composition (x=0.73, y=0.6) which is lattice-matched to InP and has a room-temperature band gap of 0.96 eV, since this particular composition has been suggested as being suitable for microwave device applications [1].

Transient velocity calculations have not been reported for the quaternary, and the concept of velocity overshoot could become very important for devices with submicron active dimensions. It will be shown in this paper that the Γ-valley effective mass is of basic importance in determining the nature of the velocity-overshoot characteristics of $Ga_{1-x}In_xP_{1-y}As_y$. One primary reason is that this quaternary is a material which, to a large extent, is dominated by scattering in the central valley due to the predicted large Γ-L intervalley energy separation [11].

The static velocity-field calculations have been described previously [1]. In the transient analysis procedure, electrons are randomly selected from a Maxwellian velocity distribution with T=300°K. The electric field intensity is independent of position. Each electron undergoes

scattering as it would in a single-electron monte carlo procedure. During the drift, the instantaneous velocity and position of the electron are recorded at specific times over a time interval generally long enough to allow the particle to reach a steady-state velocity. This procedure is then repeated N times (N=5000), and the instantaneous ensemble-averaged velocity and distance along the field direction are calculated as a function of the time. The data presented here will be in the form of velocity versus distance since this gives a more qualitative assessment of the persistence of velocity overshoot in terms of physical device dimensions.

Figure 1 shows the static velocity-field characteristic for $Ga_{.27}In_{.73}P_{.4}As_{.6}$ for two values of Γ-valley effective mass, along with a curve for GaAs. The carrier density is $1x10^{17}cm^{-3}$. The effective mass of 0.036 m_o for the quaternary is obtained from the interpolation procedure [1,8], while the value of 0.05 m_o is chosen based on the more recently-measured values [7,10]. The calculation includes alloy scattering for the quaternary and assumes a random alloy with no sublattice ordering [1,12]. The increased Γ-valley effective mass decreases the drift mobility of the quaternary from 7000 cm^2/volt sec to 4900 cm^2/volt sec, which is very close to the GaAs value. The peak velocity is still larger than for GaAs at this doping level, although the threshold field is also larger. The peak-to-valley ratio, with the valley velocity taken at 20 kV/cm, is nearly the same for GaAs and the quaternary with $m^*(\Gamma)=0.05\ m_o$. Also shown in Figure 1 is the velocity-field characteristic for the quaternary with $m^*(\Gamma)=0.05\ m_o$ without alloy scattering. Alloy scattering is more detrimental to the static velocity-field curve for this value of

effective mass than for the value of 0.036 m_o [1]. Some of the recent experimental transport property data does indicate that a scattering mechanism having a temperature dependence of mobility the same as alloy scattering is greatly affecting the electron dynamics. The problem of alloy scattering in the quaternary material remains as a major barrier to the realization of many of the potentially useful material properties.

Figure 2 shows the velocity versus distance characteristic for the quaternary both with and without alloy scattering for effective mass values of 0.036 m_o and 0.05 m_o and a constant field of E=10 kV/cm. Shown for comparison is a curve for GaAs, which is in very good agreement with results calculated by other authors [13-15]. Figure 3 shows similar calculations for a field of 25 kV/cm. There are several points to be made. For an effective mass of 0.036 m_o the velocity-overshoot is very dramatic, and even including the effects of alloy scattering it persists over distances of greater than approximately 0.35 μm. For an effective mass of 0.05 m_o the velocity overshoot is much reduced and for small distances ($<$0.3 μm) the instantaneous velocity for GaAs is greater than that for the quaternary with alloy scattering. It should be pointed out that due to the shift of the threshold field in the quaternary with $m^*(\Gamma) = 0.05\ m_o$ to about 8 kV/cm, one would expect a very small amount of velocity overshoot for fields only slightly above the threshold field [13-15], as is the case in Figure 2. The effect of alloy scattering on the velocity overshoot for $m^*(\Gamma) = 0.05\ m_o$ is considerably larger than that for $m^*(\Gamma) = 0.036\ m_o$. It can be seen that both alloy scattering and central valley effective mass are predicted to have a significant effect on the velocity overshoot characteristic for this quaternary alloy,

and the actual values of parameters used in the simulation will determine whether or not $Ga_{1-x}In_xP_{1-y}As_y$ is far superior to GaAs or is only comparable to GaAs.

Recently, it has become apparent that new physical concepts could be involved in the electron dynamics in sub-micron device structures [16]. Also, it is obvious that for real devices, such as in the channel region of a micron-geometry MESFET, the electric field intensity is not constant and varies drastically with position in the channel. The spatial variation of electric field will play a significant role in the influence of electron dynamics on device performance. Thus, calculations such as those presented here and elsewhere [13-16] can only be taken as the first step in assessing the magnitude of the velocity-overshoot effect. By comparing two materials in the manner presented here, one can assess the relative performance of the quaternary in comparison to GaAs. Based upon the work presented here there still appear to be reasons for being optimistic about the potential of $Ga_{1-x}In_xP_{1-y}As_y$ as a microwave material. However, as these results demonstrate any definite conclusions must await further experimental evaluation of the exact material parameters of the quaternary.

List of Figures

List of References

1) LITTLEJOHN, M.A., HAUSER, J.R., and GLISSON, T.H., "Velocity field characteristics of $Ga_{1-x}In_xP_{1-y}As_y$ quaternary alloys", Appl. Phys. Lett., 1977, 30 (5), pp. 242-244.

2) MOON, R.L., ANTYPAS, G.A., and JAMES, L.W., "Bandgap and lattice constant of GaInAsP as a function of alloy composition", J. Electron. Mater., 1974, 3 (10), pp. 635-647.

3) GLISSON, T.H., HAUSER, J.R., LITTLEJOHN, M.A., AND WILLIAMS, C.K., "Energy bandgap and lattice constant contours of III-V quaternary alloys", J. Electron. Mater., 1978, 7 (1), pp. 1-15.

4) NAHORY, R.E., POLLACK, M.A., JOHNSTON, W.D.,JR., and BARNS, R.L., "Band gap versus composition and determination of Vegard's law for $In_{1-x}Ga_xAs_yP_{1-y}$ lattice-matched to InP", Appl. Phys. Lett., 1978, 33 (7), pp. 659-661.

5) RESTORFF, J.B., HOUSTON, BLAND, BURKE, J.R., AND HAYES, R.E., "Measurement of effective mass in $In_{.9}Ga_{.1}As_{.22}P_{.78}$ by Shubnikov-de Haas oscillations", Appl. Phys. Lett., 1978, 32 (3) pp. 189-190.

6) NISHINO, T., YAMAZOE, Y., and HAMAKAWA, Y., "Electroreflectance in $In_{0.79}Ga_{0.21}As_{0.54}P_{0.46}$", Appl. Phys. Lett., 1978, 33 (10), pp. 861-862.

7) NICHOLAS, R.J., PORTAL, J.C., HOULBERT, C., PERRIER, P., and PEARSALL, T.P., "An experimental determination of the effective masses for $Ga_{1-x}In_xAs_yP_{1-y}$ alloys grown on InP", Appl. Phys. Lett., 1979, 34 (8), pp. 492-494.

8) LITTLEJOHN, M.A., SADLER, R.A., GLISSON, T.H., and HAUSER, J.R., "Carrier compensation and alloy scattering in $Ga_{1-x}In_xP_{1-y}As_y$ grown by liquid-phase epitaxy", Inst. Phys. Conf. Ser., 1979, 45, pp. 239-247.

9) LEHENY, R.F., BALLMAN, A.A., DeWINTER, J.C., NAHORY, R.E., and POLLACK, M.A., "Compositional dependence of the low field mobility in $In_{1-x}Ga_xAs_yP_{1-y}$", Abstract L-3, presented at the 21st Electronic Materials Conference, Boulder, CO, June 27-29, 1979.

10) PEREA, E.H., MENDEZ, E., and FONSTAD, C.G., "Electron effective mass in $In_uGa_{1-u}P_vAs_{1-v}$ for $0 \leq v \leq 1$", Abstract L-4, presented at the 21st Electronic Materials Conference, Boulder, CO, June 27-29, 1979.

11) HAUSER, J.R., GLISSON, T.H., and LITTLEJOHN, M.A., "Negative resistance and peak velocity in the central (000) valley of III-V semiconductors", Solid-State Electron., 1979, in press.

12) LITTLEJOHN, M.A., HAUSER, J.R., GLISSON, T.H., FERRY, D.K., and HARRISON, J.W., "Alloy scattering and high field transport in ternary and quaternary III-V semiconductors", Solid-State Electron., 1978, 21 (1), pp. 107-114.

13) RUCH, J.G., "Electron dynamics in short channel field effect transistors", IEEE Trans. Electron Dev., 1972, ED-19 (5), pp. 652-654.

14) MALONEY, T.J., and FREY, J., "Transient and steady-state electron transport properties of GaAs and InP", J. Appl. Phys., 1977, 48 (2), pp. 781-787.

15) KRATZER, S., and FREY, J., "Transient velocity characteristics of electrons in GaAs with Γ-L-X conduction band ordering", J. Appl. Phys., 1978, 49 (7), pp. 4064-4068.

16) BARKER, J.R., and FERRY, D.K., "On the physics and modeling of small semiconductor devices, I and II", Solid-State Electron., 1979, in press.

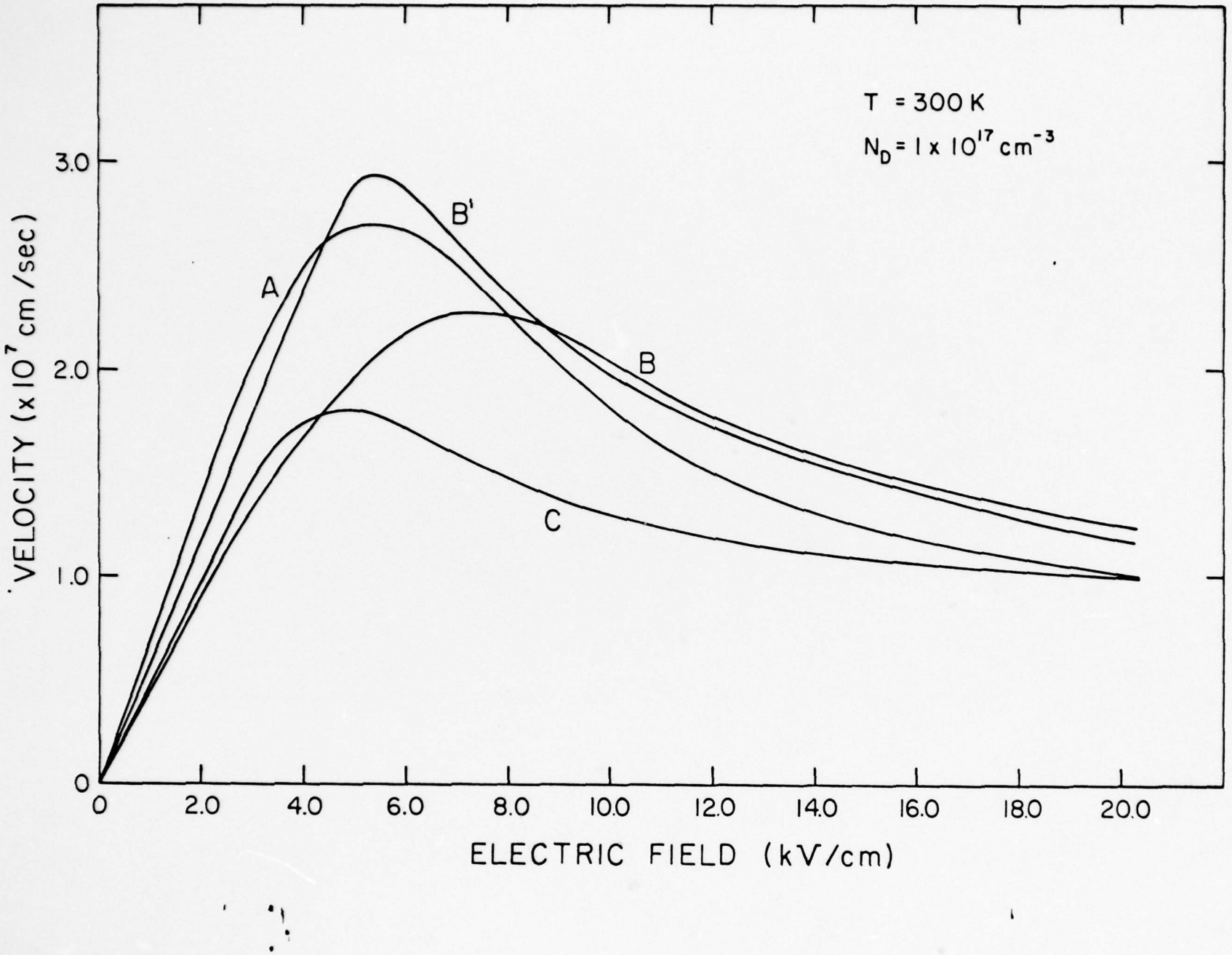
T = 300 K
$N_D = 1 \times 10^{17}\ cm^{-3}$
A
B'
B
C
VELOCITY ($\times 10^7$ cm/sec)
3.0
2.0
1.0
0
0
2.0
4.0
6.0
8.0
10.0
12.0
14.0
16.0
18.0
20.0
ELECTRIC FIELD (kV/cm)

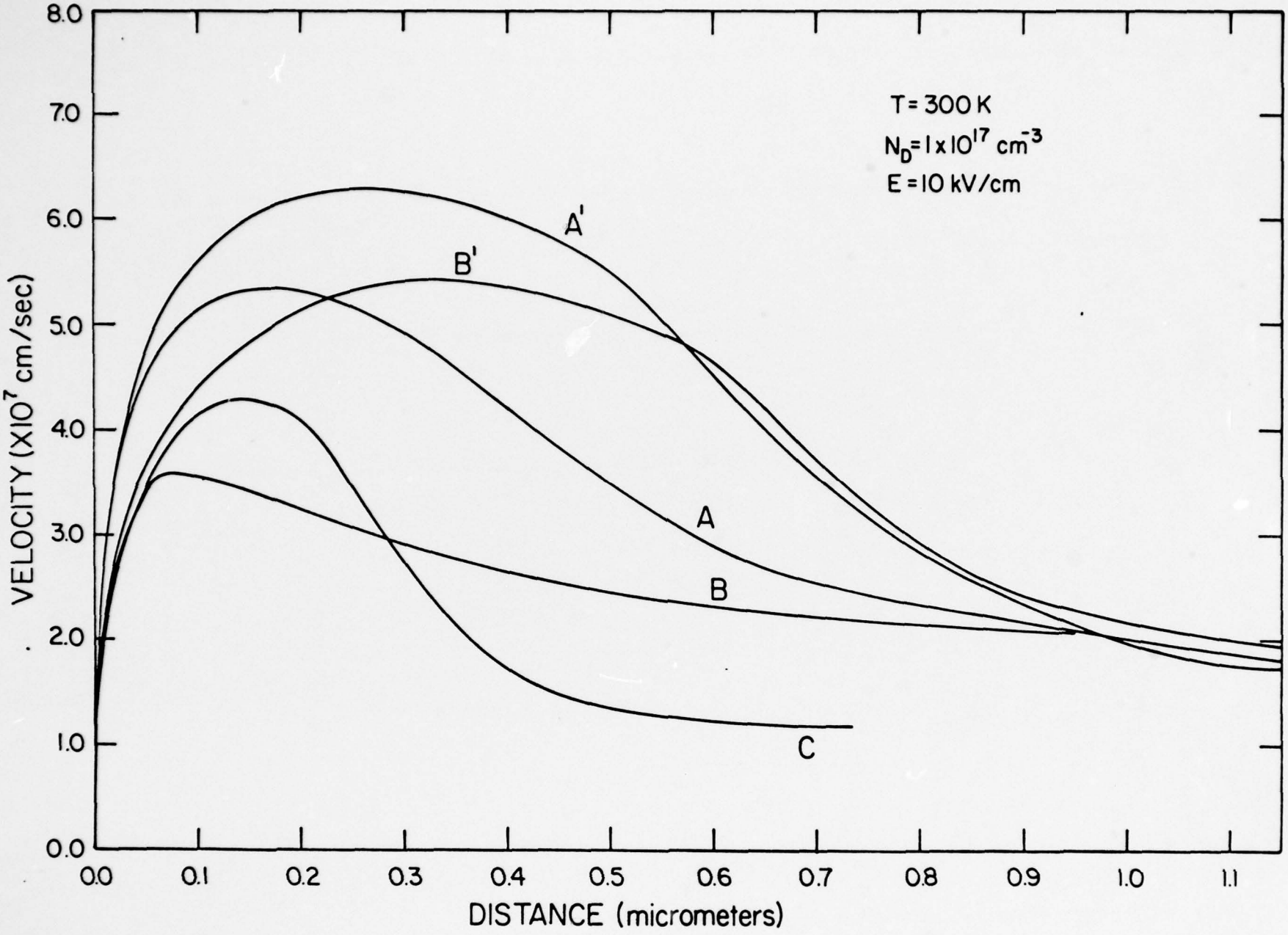
T = 300 K
$N_D = 1 \times 10^{17}$ cm^{-3}
E = 10 kV/cm
A'
B'
A
B
C
VELOCITY (X10^7 cm/sec)
DISTANCE (micrometers)
8.0
7.0
6.0
5.0
4.0
3.0
2.0
1.0
0.0
0.0
0.1
0.2
0.3
0.4
0.5
0.6
0.7
0.8
0.9
1.0
1.1

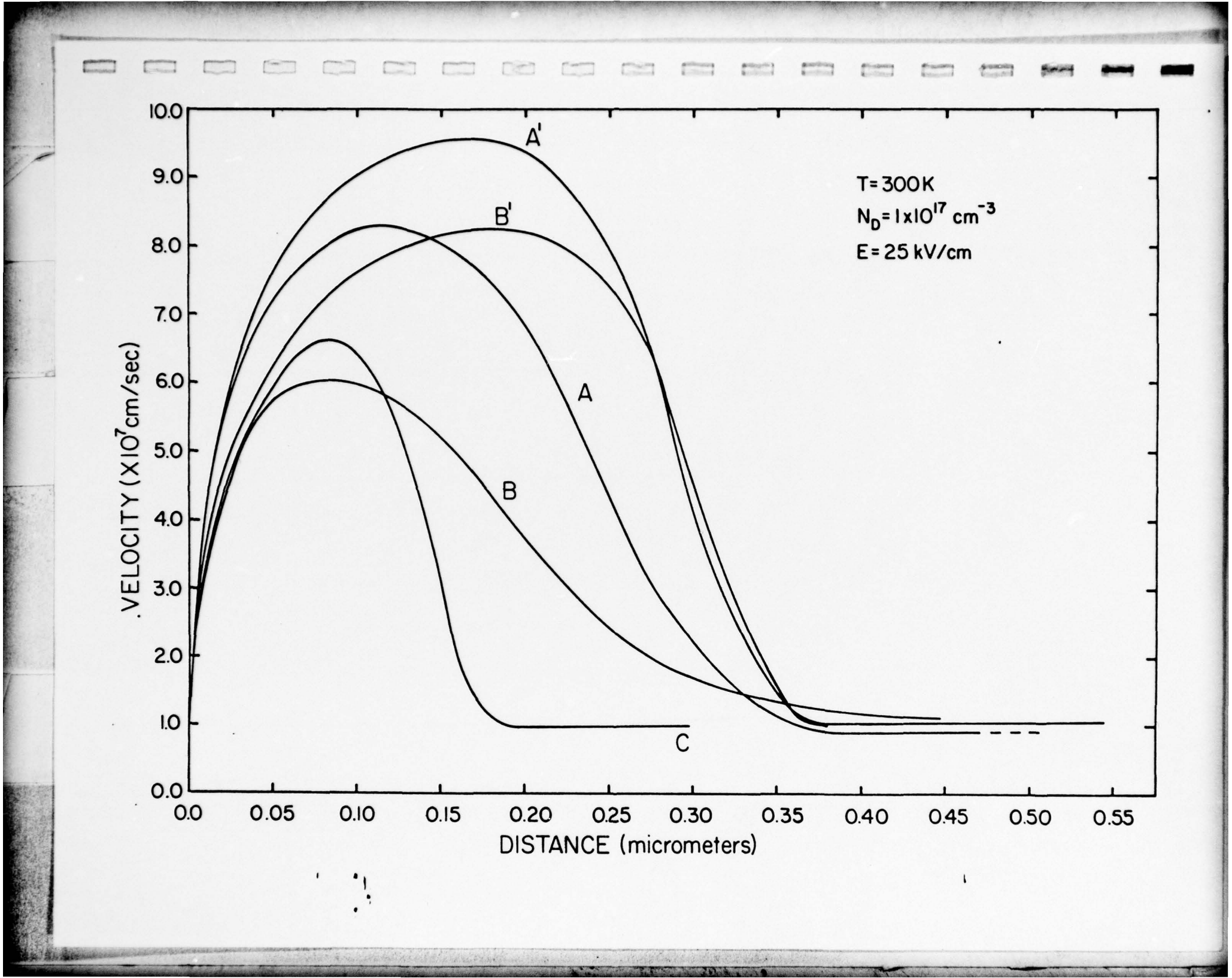
T=300K
$N_D = 1 \times 10^{17}$ cm^{-3}
E=25 kV/cm
A'
B'
A
B
C
VELOCITY (X10^{7}cm/sec)
DISTANCE (micrometers)
10.0
9.0
8.0
7.0
6.0
5.0
4.0
3.0
2.0
1.0
0.0
0.0
0.05
0.10
0.15
0.20
0.25
0.30
0.35
0.40
0.45
0.50
0.55

ANNUAL REPORT DISTRIBUTION LIST

Contract N00014-76-C-0480

Office of Naval Research
Arlington, VA 22217
Attn: Code 427 (4)
Code 102IP (6)

Defense Documentation Center (12)
Building 5
Cameron Station
Alexandria, VA 22314

Naval Research Laboratory
Washington, DC 20375
Attn: Code 2627 (6)
Code 5220 (1)
Code 5211 (1)

Naval Ocean Systems Center
San Diego, CA 92152
Attn: H. Wieder, Code 922 (1)

Varian Associates
Palo Alto, CA 94303
Attn: R. Bell, Box K101 (1)

RCA Laboratories
David Sarnoff Research Center
Princeton, NJ 08540
Attn: Dr. Y. S. Narayan (1) (1)

TRW Defense and Space Systems Group
One Space Park
Redondo Beach, CA 90278
Attn: Dr. T. Mills (1)

Motorola
5005 E. McDowell Street
Pheonix, AZ 85008
Attn: T. S. Heng (1)

Raytheon Company
28 Seyon Street
Waltham, MA 02154
Attn: R. Berig (1)

Westinghouse Research Lab
Beulah Road
Pittsburgh, PA 15235
Attn: H. C. Nathanson (1)

Rockwell International
Science Center
1049 Camino Dos Rios
P. O. Box 1085
Thousand Oaks, CA 91360
Attn: Daniel Chen (1)

Hughes Research Laboratories
Malibu Canyon Road
Malibu, CA 90265
Attn: C. Krumm (1)

Washington University
St. Louis, MO 63130
Attn: Prof. C. M. Wolfe (1)

Texas Instruments
Mail Stop 118
P. O. Box 5012
Dallas, TX 75222
Attn: D. Shaw (1)

University of Illinois
Urbana, IL 61801
Attn: G. E. Stillman (1)